AD-A118 800 NORTH CAROLINA STATE UNIV RALEIGH DEPT OF MATERIALS --ETC F/G 20/2
SINGLE CRYSTAL EPITAXY AND CHARACTERIZATION OF BETA-SIC.(U)
JUL 82 R F DAVIS N00014-79-C-0121
UNCLASSIFIED 243-027-013 NL

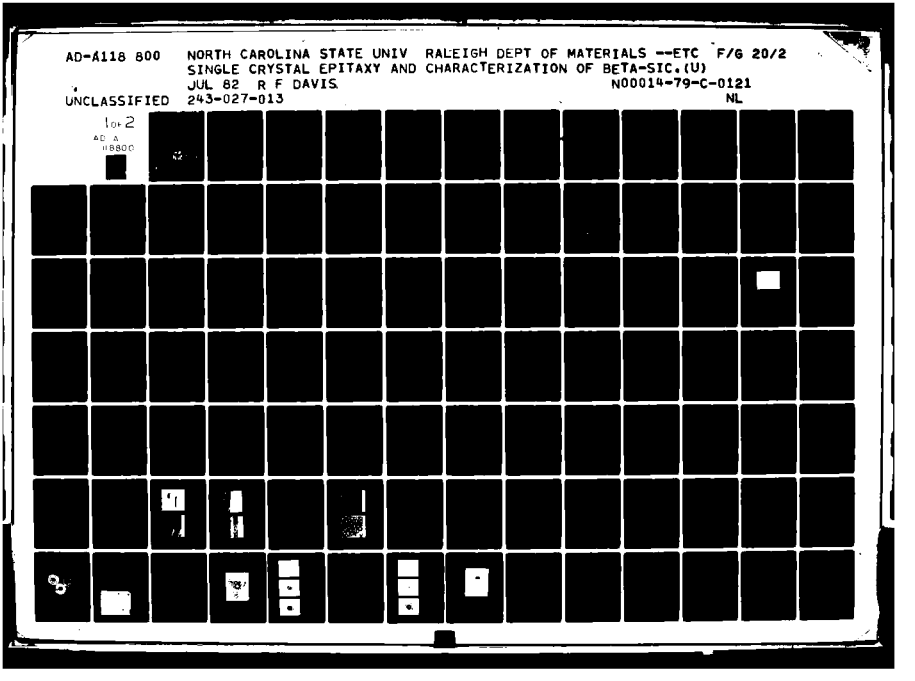

(12)

School of Engineering
North Carolina State University
Raleigh, North Carolina

12

Materials Engineering Department
109 Page Hall
North Carolina State University
Raleigh, NC 27650

Final Technical Report

on

SINGLE CRYSTAL EPITAXY AND CHARACTERIZATION OF β-SiC

Supported by ONR under Contract N00014-79-C-0121

July 1982

Report #243-027-013

Principal Investigator:

Professor R. F. Davis
Materials Engineering Department

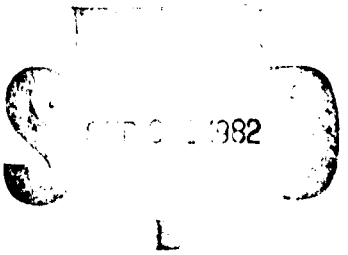

SECURITY CLASSIFICATION OF THIS PAGE (When Data Entered)

REPORT DOCUMENTATION PAGE

READ INSTRUCTIONS BEFORE COMPLETING FORM

1. REPORT NUMBER: 243-027-013	2. GOVT ACCESSION NO.: AD-A118800
3. RECIPIENT'S CATALOG NUMBER:	
4. TITLE (and Subtitle): Single Crystal Epitaxy and Characterization of β-SiC	5. TYPE OF REPORT & PERIOD COVERED: Annual Report 1 Jan '81 - 31 Dec '81
	6. PERFORMING ORG. REPORT NUMBER:
7. AUTHOR(s): R. F. Davis	8. CONTRACT OR GRANT NUMBER(s): N00014-79-C-0121
9. PERFORMING ORGANIZATION NAME AND ADDRESS: Materials Engineering Department, North Carolina State University, 109 Page Hall, Raleigh, NC 27650	10. PROGRAM ELEMENT, PROJECT, TASK AREA & WORK UNIT NUMBERS: PE 61153N, RR 021-02-03, NR 243-027
11. CONTROLLING OFFICE NAME AND ADDRESS: ONR-427, Arlington, VA 22217	12. REPORT DATE: June 30, 1982
	13. NUMBER OF PAGES: 97
14. MONITORING AGENCY NAME & ADDRESS(if different from Controlling Office)	15. SECURITY CLASS. (of this report): Unclassified
	15a. DECLASSIFICATION/DOWNGRADING SCHEDULE

16. DISTRIBUTION STATEMENT (of this Report)

Approved for public release; distribution unlimited

17. DISTRIBUTION STATEMENT (of the abstract entered in Block 20, if different from Report)

18. SUPPLEMENTARY NOTES

ONR Scientific Officer; Tel: (202) 696-4218

19. KEY WORDS (Continue on reverse side if necessary and identify by block number)

Silicon Carbide	R-F Sputtering
Crystal Growth	Phase Equilibria
Vapor Phase Epitaxy	Thermodynamics

fefa

20. ABSTRACT (Continue on reverse side if necessary and identify by block number)

Epitaxial thin films of β-SiC of up to five microns in thickness have been reproducibly grown on (100) and (111) Si single crystal wafers. A two-step process involving the initial chemical conversion of the Si surface to SiC using C_2H_4 alone followed by direct CVD of SiC using both SiH_4 and C_2H_4 was employed to achieve this objective. Theoretical CVD phase diagrams for the Si-C-H and Si-C-Ar system have been calculated for various reactive gases, Si/Si+C ratios, temperatures and total pressures. Amorphous SiC has also been produced using a remodeled rf sputtering unit.

DD FORM 1 JAN 73 1473 EDITION OF 1 NOV 65 IS OBSOLETE
S/N 0102-014-6601

Enclosure (1)

SECURITY CLASSIFICATION OF THIS PAGE (When Data Entered)

TABLE OF CONTENTS

I. Introduction

Silicon carbide is the only compound species that exists in the solid state in the Si-C system and can occur in the cubic (C), hexagonal (H) or rhombohedral (R) structures. It is also classified as existing in the beta and alpha modifications. The beta, or cubic, form crystallizes in the zincblende or sphalerite structure; whereas, a large number (approximately 140) of the alpha occur in the hexagonal or rhombohedral forms known as polytypes.

Because of the emerging need for high temperature, high frequency and high power electric devices, blue L.E.D.'s, Schottky diodes, U.V. radiation detectors, high temperature photocells and heterojunction devices, silicon carbide is being examined throughout the world for employment as a candidate material in these specialized applications. The electron Hall mobility of high purity undoped β-SiC is approximately a factor of three larger (~1000 $cm^2/v\text{-}sec$) than that of the α-form over the temperature range of 300-1000K because of the smaller amount of phonon scattering in the cubic material. The energy gap is also less in the β form (2.3 eV) compared to the α-forms (e.g., 6H = 2.86 eV). Thus, the β-form is now considered more desirable for electronic device applications, and, therefore, the growth of thin films of this material constitutes the principle objective of this research program. Unfortunately, the earlier push in the 1956-1970 time span to develop SiC as an electronic material concentrated heavily on high temperature growth processes such as the Lely sublimation-condensation technique which produced a variety of α polytypes in experiments which were rarely reproducible. Toward the end of this initial thrust, techniques such as chemical vapor deposition (CVD), sputtering, traveling solvent and solution growth showed promise not only as techniques per se but as experimental avenues wherein the growth of β-SiC could be achieved.

The primary objective of the present research program was to capitalize on and extend the knowledge of the CVD and sputtering processes that were discerned not only in the brief initial efforts with SiC, but that have also been developed for these processes in the intervening years in research on other semiconductor materials.

To this end, excellent quality single crystal thin films of β-SiC have been successfully grown using specially designed and very closely controlled variable pressure chemical vapor deposition (C.V.D.) equipment. The growth of an epitaxial β-SiC film on Si (111) and Si (100) was found to be reproducible if a two-step process was employed. This method entailed the initial chemical conversion of the Si surface through the use of C_2H_4 alone. This step was followed by direct and continual deposition of SiC via the separate decomposition of SiH_4 and C_2H_4 on the converted layer.

In addition, an adjustable target r-f sputtering unit with separately controlled gas input and pressure regulation has been redesigned around an older commercial unit. The primary goal of this second task was to produce amorphous layers of SiC which can be used as substrates for the C.V.D. effort. Finally, a separate but a very important and an over-lapping research program involving the computer-assisted calculation of C.V.D phase diagrams from basic thermodynamic data in the Si-C system has been completed. The details of these efforts and the results are reported below.

II. Review of Selected Prior Research Programs in SiC

A. Chemical Vapor Deposition Reactions and Thermodynamics

Chemical vapor deposition is a material synthesis method in which the constitutents of the vapor phase react to form a solid film at a heated surface. Various chemical reactions with widely different free energy changes and activation energies can usually be caused to occur for the growth of a given material by the judicious selection of the appropriate gases. However, the chemical reaction chosen for the growth process should be thermochemically and kinetically favorable.

The ability to model a CVD system so that the behavior of the system is predictable is quite valuable. Unfortunately, the total CVD process is very complex, involving chemical thermodynamics, chemical kinetics, as well as mass and heat transfer phenomena. Many CVD systems also have unique properties, such as the configuration of the substrates and temperature gradients in the reactor, which affect the deposition and make the development of general models difficult. Chemical thermodynamic equilibrium calculations, however, are useful for determining limiting rates of deposition and for indicating appropriate CVD conditions.

A perusal of the literature has revealed that numerous methods have been reported for computing thermodynamic equilibrium compositions and that essentially all the techniques have been based on the methods of either Brinkley (1, 2) or White, et al. (3). The former requires the writing of a series of chemical reactions and the computation of their respective equilibrium constants; whereas, the latter involves minimizing the summation of the free energies of all species.

Only a few researchers have used thermodynamic equilibrium calculations to predict the phases which will form during the CVD of SiC. Lewis (4) has calculated, based on White's method, the equilibrium concentrations for the C-Cl-H-Si system to explain the formation of SiC from methyltrichlosilane (CH_3SiCl_3) in H_2 at atmospheric pressure and 1427°C. A metastable intermediate stage involving the formation of Si and C was proposed in assessing the free energy change of the surface reaction. At a state of full thermodynamic equilibrium, gaseous

chlorosilanes and hydrocarbons at their metastable concentrations react together to precipitate SiC. Equilibrium gas concentrations for this metastable stage and for the final equilibrium stage were calculated and plotted as a function of the partial pressure of CH_3SiCl_3 at one atmosphere total pressure and 1427°C. According to the phase rule, in a four-component system with the variables T. P. and Cl/H ratio fixed, three phases (one gaseous and two condensed) are allowed. Therefore, only two out of the three possible condensed phases (Si, C and SiC) were selected in each computation. The resulting condensed phases were SiC + C and SiC alone under the aforementioned equilibrium conditions. The second phase of C occurs because of the presence of Cl atoms in the equilibrium system which react with Si to form various chlorosilanes or Si chlorides. As a result, this makes the ratio of Si/C which is available to form condensed phase equal to a value ≤ 1.

Minagwa and Gatos (5) have presented equilibrium computations for the growth by CVD of α-SiC from silane (SiH_4) and propane (C_3H_8) in H_2 or an inert gas atmosphere. Beta SiC was not considered in their calculations because α-SiC substrates were used for the epitaxial growth. These investigators assumed that the structure of the substrates controls the structure of the growing layer in this system which was found to be experimentally true in subsequent research.

The computation procedure used by these investigators was based on that developed by Cruise (6). A total of thirty species was included in the computation. However, solid Si was not included because the temperature range considered was above the melting temperature of this element. The deposition ranges of the condensed species were plotted as a function of the partial pressure of C_3H_8 against that of SiH_4 in 100°C increments between 1427°-1827°C. In a H_2 atmosphere, the deposition of single phase α-SiC occurs over a wide range of reactant partial pressure, i.e., from $P(SiH_4) = 3P(C_3H_8)$ to an even greater excess of C_3H_8. In an inert gas atmosphere, this range is limited to the vicinity of $P(SiH_4) = 3P(C_3H_8)$, i.e., equal concentrations of Si and C in the reactant gas. This difference is attributed to the fact that the inert gas can not react with the excess C in the vapor phase.

Therefore, a precise control of the Si/C ratio is required to ensure a single phase deposition in an inert gas system. However, this inert gas system may have an advantage over the H_2 atmosphere in that H_2 etches SiC, albeit slowly, at temperatures above 1550°C (51). As a result, the growth rate is expected to be higher in the inert gas atmosphere.

Harris et al. (7) have computed the equilibrium concentrations of a total of 30 species in the Si-C-H system from 1300°-2000°C with a program based on White's method. It has been noted by these investigators that this type of computation gives no information as to how the condensed phases physically coexist, which polytypes are formed, and whether or not the SiC appears in single-crystal or polycrystalline form. Therefore, SiC was included as a general condensed form, and no distinction was made between the α and β forms. However, from an experimental viewpoint, Harris et al. found that single-crystalline α-SiC was consistently obtained on α-SiC substrates over the whole imput concentration range for which SiC is the only thermodynamically stable condensed phase. Polycrystalline layers of varying morphology were invariably obtained under conditions corresponding to the two-phase (either SiC + Si or SiC + C) regions. In this respect, the computed results were found to be in reasonable agreement with experimental data.

The single phase SiC region was also found to be wider at the lower input concentrations of Si and C for a given fixed amount of H_2 because significant amounts of C can be retained in the vapor phase as various hydrocarbons. Therefore, stoichiometric SiC can be formed at Si/C input concentration ratios varying from 0.21 to 0.89. From this conclusion, it is clear that using H_2 as carrier gas will provide one more control parameter in the CVD of SiC.

Eriksson (8) has extended White et al.'s method to include systems containing more than one condensed phase and has developed a computer program, SOLGAS, for performing the calculations. He has subsequently modified the program (9, 10) into SOLGASMIX so that condensed solution phases can also be considered. To prevent the omission of an important

species, the programs can consider all conceivable gaseous species and condensed phases of invariant or variable stoichiometry and mixtures at constant total pressure and temperature in a single calculation. Unstable condensed phases are rejected from the calculation. This program can also handle non-ideal phases, provided activity coefficient relationships are available. Finally, Bessman and Spear (11) have produced a new version of the program (SOLGASMIX-PV) which incorporates the ideal gas law. This last version is now capable of calculating equilibra at a constant total gas volume with variable total pressure.

An effort is made in this research to explore the thermodynamic equilibrium compositions of the Si-C-H system by the aforementioned SOLGASMIX-PV program. The results of these calculations will be presented in the RESULTS AND DISCUSSION section.

B. Thin Film Formation of Beta Silicon Carbide by Vapor Deposition

Brander (12) has reviewed the vapor phase epitaxial growth of SiC up to 1973. A recent and more complete review of the various CVD conditions for the deposition of SiC on different substrates has been presented by Schlichting (13). In general, the two most common vapor deposition techniques for growing β-SiC thin films are chemical conversion and chemical vapor deposition. Some of the previous research concerned with these processes will be reviewed in this section.

1. Chemical Conversion of Silicon to Beta Silicon Carbide

Generally the substrate plays a rather passive role in the vapor deposition process. Unless the substrate material is totally different in composition from the constituents of the deposit, it is difficult to detect the introduction of foreign atoms from the substrate material in the film. In some cases, however, it may be desirable for the substrate to take part in the reaction. This may be considered as a special case of CVD, and is frequently termed "chemical conversion."

Chemical conversion in the case of β-SiC formation is the reaction of single crystal Si substrates with a C-containing gas (usually a hydrocarbon gas) at elevated temperatures. This technique is in essence a "carburization" process. It can be separated into two types

according to the growth technique employed: 1) reaction of the Si substrate with a hydrocarbon gas contained in a flowing gas mixture under conditions of viscous flow[*1] (14-18), and ii) reaction at the Si substrate surface in high (HV)[*2] or ultra-high (UNV)[*3] vacuum chambers at a hydrocarbon partial pressure corresponding to (free) molecular flow[*4] (19-24).

Various hydrocarbons such as C_2H_2 (19, 20, 22-24), C_2H_4 (19-21), C_3H_8 (18), and CH_4 (14-17),[*5] or even the graphite susceptor (regular and pyrolytic) (25) have been used as the C source to convert a Si substrate surface into β-SiC. Saturated hydrocarbons[*6] (e.g., CH_4 and C_3H_8) have been used in the first technique, which requires temperatures in excess of 1100°C at a total pressure near 1 atm, while unsaturated hydrocarbons[*7] (e.g., C_2H_4 and C_2H_2) have been used in the second technique, in which temperatures as low as 800°C may be employed under HV or UHV conditions. The substantially lower

---

*1 The flow regime can be determined by Knudsen's number, $Kn = \lambda/d$ where λ = the mean free path of the gas atoms in the system and d = the minimum physical dimensions of the system. A viscous flow condition occurs when $Kn \ll 1$ in a system. The character of the gas flow in this regime is determined by gas-gas collisions.

*2 High vacuum is defined as the pressure in the $1-10^{-3}$-10^{-6} Torr range. This term is also used in a broader sense to designate any environment with a pressure smaller than 10^{-3} Torr.

*3 Ultrahigh vacuum is defined as any pressure below 10^{-9} Torr.

*4 The condition of (free) molecular flow occurs when $Kn > 1$ in a system. The flow properties in this regime are determined by gas-wall collisions. (Note: The transition from viscous flow to molecu-flow and vise versa, is not sharp but gradual. Therefore, when $0.01 < Kn < 1$ the flow condition is termed "transition flow.")

*5 C_2H_2 = acetylene, C_2H_4 = ethylene, C_3H_8 = propane and CH_4 = methane.

*6 Saturated hydrocarbons are organic compounds containing no double or triple bonds between C atoms.

*7 Unsaturated hydrocarbons are organic compounds containing double or triple bounds between C atoms.

growth temperature for the vacuum growth environment than for the near atmospheric pressure environment is because of i) the unsaturated hydrocarbon decomposes relatively easy and at lower temperatures, and ii) the vacuum condition enhances the decomposition of the hydrocarbon as well as the desorption of H_2 produced on the growing surface in the absence of a H_2 carrier gas.

Mayer and Gomer (25) have noted that hydrocarbon gases do not decompose on a hot surface when the gas pressure is so low that the mean free path exceeds the dimensions of the reaction chamber (i.e., under the condition of molecular flow). This is for saturated hydrocarbons (e.g., CH_4 and C_3H_8) which decompose endothermically, but is not the case for unsaturated hydrocarbons (e.g., C_2H_4 and C_2H_2) which decompose exothermically. The complete decomposition of saturated hydrocarbons requires numerous gas-gas collisions to form stable intermediates. A larger mean free path under vacuum conditions for the chemical conversion of Si to form β-SiC. However, unsaturated hydrocarbons can decompose under vacuum because the breaking of double or triple C bonds is relatively easy. The results of Khan and Summergrad (19) have indicated that unsaturated hydrocarbons such as C_2H_4 and C_2H_2 are the most favorable C-containing gases for the chemical conversion of Si to β-SiC in vacuum within the temperature range of 300°-1000°C. The above authors have also noted that CO, CO_2 and CH_4 yield no detectable β-SiC film growth at temperature up to 1000°C.

Tombs et al. (26) have grown highly adherent epitaxial films of β-SiC on single crystal Si substrates by heating in the presence of a graphite susceptor in a one atmosphere Ar ambient. In their study, both spectrographic grade graphite and pyrolytic graphite were used as susceptor materials and as C sources at an estimated Si surface temperature of 1250°C (uncorrected optical pyrometer reading). Other possible C sources either from the impurities in the Ar gas or from the gases trapped in the graphite susceptor were eliminated by titanium sponge purification of the Ar gas and by the outgassing of the graphite susceptor prior to the loading of the Si substrates. The grown β-SiC film has monocrystalline layers near the final grown surface and polycrystalline layers near the Si/SiC interface. The formation of β-SiC

layers proceeded at a much slower rate when pyrolytic graphite was employed as the susceptor. The exact reasons for this are not known.

It is important to note at this point the importance of eliminating the SiO_2 film on the Si substrate surface prior to the chemical conversion process, because the reaction of SiO_2 with all hydrocarbon gases to form SiC is thermodynamically extremely unfavorable. Three different etching methods have been used by various investigators to eliminate SiO_2: i) HF acid chemical etching prior to loading (14, 24), ii) *in-situ* thermal etching at temperatures above 1000°C in a flow of either H_2 or He prior to conversion (17, 24), and iii) *in-situ* HCl vapor etching prior to conversion (15, 24). The first method does eliminate the SiO_2; however, the Si surface oxidizes again as soon as it leaves the acid no matter how quick it is transferred to the reaction chamber. *In-situ* thermal etching in a H_2 flow at higher than 1000°C temperatures has caused degradation in the smoothness of the Si surface. This is believed (27) to be caused by the H_2 reduction of SiO_2 layers. Balog et al. (17) have concluded that a smooth Si surface can be produced after a 10 min. thermal etch in a flow of He gas. The best etching method for Si is considered to be the *in-situ* HCl vapor etching, because it etches away not only the SiO_2 layer but also any surface damage introduced during mechanical polishing of the wafer. However, the proper combination of the HCl concentration in H_2 and the etching temperature needs to be followed to ensure a smooth surface.

The microstructure of the β-SiC films grown by Si conversion in systems wherein the flowing hydrocarbon and carrier gas is in the viscous flow regime may be either a completely polycrystalline structure (14, 16, 18) or single crystal in nature only at the β-SiC/Si interface. Usually, the latter graduates into a polycrystalline layer after several additional Å of deposit (15, 25). Nakashima et al. (15) claimed but did not confirm that single crystal films could be obtained using CH_4 in an carrier when the film thickness remained below 1000 Å. Similarly, thin single crystal films having a thickness of about 400 Å have been reported by Balog et al. (17) at their highest growth

temperature of 1350°C using CH_4 in He, while films grown at lower temperatures were found to be polycrystalline.

Epitaxial films grown in both MV and UHV systems wherein an unsaturated hydrocarbon gas flow corresponds to free molecular flow exhibit characteristic "pit" and "hillock" type defects (19-24), in addition to the usual crystallographic defects (stacking faults, twins, etc.) commonly found in thin epitaxial films. With higher partial pressures of hydrocarbon gases (e.g., $C_2H_2 > 10^{-5}$ Torr) in the reaction chamber, these pits and hillocks can be sealed as a result of the higher growth rate at an early stage in the growth process (24). Subsequent growth, however, is nearly completely suppressed as a result of the impermeability of the SiC product layer to the diffusion of Si (see the following discussion).

Nakashima et al. (15) and Tombs et al. (25) have proposed that the conversion reaction occurs at the Si/β-SiC interface by inward diffusion of the C species because of its small size. However the growth mechanism has also been investigated by Graul and Wagner (16) using a ^{14}C tracer method. This latter set of experiments showed that the growth of the SiC layer is actually caused by diffusion of Si through the growing SiC layer to the outer reaction surface. Mogab and Leamy (24) have concluded that the porous defect regions of the film provide a rapid "short circuit" path for the out-diffusion of Si to the surface. Therefore, the rate of supply of Si will vary with the quality and the grain size of the SiC layers.

Besides the single-step process, i.e., the direct reaction of a given hydrocarbon gas with a Si substrate in a temperature higher than 1200°C, a two-step process has also been employed by investigators using CH_4 in He (17) or C_3H_8 in H_2 (18) at 1 atm. This process has been used to avoid competition between surface and volume diffusion of the Si atoms. In this method a C layer is initially deposited from the pyrolysis of a hydrocarbon gas at a moderately high temperature ($\simeq$ 900°C). This is followed by a high temperature ($\simeq$ 1200°C) anneal, which allows the reaction between Si and C to occur. Single crystal β-SiC thin films have been obtained successfully by this method. However, it has been observed by Balog et al. (17) that the growth rate

in the two-step process was appreciably slower than that in the one-step process. It has been noted (18) that prolonged annealing time and lower annealing temperature results in the formation of polycrystalline β-SiC films (sometimes with free Si). Therefore, the annealing conditions must be carefully determined for the two-step process.

In conclusion, although layers of SiC have a thickness up to 10 microns can be grown by chemical conversion, the slow Si diffusion through the film limits the thickness of good quality nonporous material to a fraction of a micron even at temperatures near the melting point of Si. To obtain thicker films of SiC, it is necessary to provide an additional source of Si by also introducing a Si-containing gas into the reaction chamber, e.g., by using the classical CVD technique.

2. Chemical Vapor Deposition of Beta Silicon Carbide

The CVD process for growing β-SiC can be divided into two basic types: single-source deposition and cqdeposition. The single source deposition processes involve the use of organosilane compounds, such as methyltrichlorosilane (CH_3SiCl_3) (28-34), dimethyldichlorosilane ($(CH_3)_2SiCl_2$) (35, 36), and diethyldichlorosilane ($(C_2H_5)_2SiCl_2$) (37), which are thermally decomposed or reduced on a heated substrate to form the SiC deposit. The codeposition processes involve the heterogeneous, reaction of mixtures of both a Si-containing gas and a C-containing gas at the heated substrate surface. Typical reactant gas combinations employed in codeposition processes have been SiH_4 and C_3H_8 (28, 38, 39), $SiCl_4$ and CH_4 (35, 40), $SiCl_4$ and C_3H_8 (40-43), $SiCl_4$ and C_6H_6 (37), $SiCl_4$ and C_7H_8 (37, 44), and $SiCl_4$ and CCl_4 (45-47). In all cases, the carrier gas employed was H_2. The total pressure was one atmosphere except for the research of Spruiell (40).

In the single-source deposition process, most people have used CH_3SiCl_3 in H_2 because the former contains Si and C in stoichiometric proportions. However, a 1:1 ratio of Si and C will not assure a pure SiC deposit. Depending upon the growth conditions, excess Si or

excess C is often found (30, 33, 34) if CH_3SiCl_3 is used. By microprobe analysis, Chin et al. (34) have shown that C-rich, stoichiometic or Si-rich SiC can be obtained using different combinations of temperature, total pressure and partial pressure of CH_3SiCl_3 partial pressure in H_2.

The codeposition processes appear to be more flexible than the single-source deposition processes. By varying the inlet gas composition and other deposition parameters such as temperature and total pressure, it should be possible to obtain deposits with controlled compositions which vary from Si-rich to C-rich. It should be noted, however, that a particular C/Si ratio provided by the two separate gases does not necessarily result in the same ration of the constituents in the deposited layer because of the different reaction kinetics and thermodynamics of the two species.

The choice of the Si-containing gas is a personal preference, because both SiH_4 and $SiCl_4$ have particular advantages and disadvantages. As far as the C-containing gas is concerned, Jackson et al. (41) have found that propane (C_3H_8) ultimately gave better results than methane (CH4). A similar conclusion was also reached by Spruiell (40). The latter author has reported that the deposition rates obtained using CH_4. However, equivalent deposits could be obtained using C_3H_8 at a temperature approximately 50°C lower than that found necessary for CH_4.

As may be inferred from the foregoing, H_2 is frequently used as the carrier gas in both single-source deposition and codeposition processes. However, Rai-Choudhury and Formigoni (35) have also used Ar as the carrier gas, and concluded that the β-SiC films deposited by the pyrolysis of $(CH_3)_2SiCl_2$ in an inert carrier gas did not show the presence of any excess Si, which was always present when the deposition was conducted in a H_2 ambient. They have explained this result by examining the different over-all reactions for each case.

The growth temperature employed by essentially all investigators using Si as the substrate falls between 1000° and 1400°C. The highest temperature is, of course, limited by the melting point of Si (1420°C).

Several other substrate materials, such as: SiC (α-SiC and β-SiC) (35, 38), sapphire (Al_2O_3) (35), Mo (45), and graphite (40), have also been used. In the codeposition process, growth temperatures as high as 1700°C have been employed if SiC was used as the substrate material. However, an even larger range of growth temperatures (1100°-2000°C) has been employed in the single-source deposition technique.

In the codeposition process using Si substrates, the growth rate of good quality β-SiC layers must, in general, be maintained lower than 0.3 μm/min. Matsunami et al. (43) have reported that a slow growth rate ($\simeq$ 0.2 μm/min.) at 1390°C favored the formation of single crystal β-SiC films on the (111), (110) and (100) planes of Si substrates. Bartlett and Mueller (28) have also found that more perfect deposits can be obtained on β-SiC substrates at the slower growth rates. By contrast, Kuroiwa and Sugano (46) employed a very slow SiC growth rate on Si(111) at between 0.007-0.017 μm/min. in the temperature range 1300°-1360°C but obtained a rough surface deposit. These investigators increased the deposition rate by raising the reactant gas concentrations in an attempt to achieve a smooth surface; however, only a polycrystalline layer was obtained. Epitaxial β-SiC films have been grown on Si(111) substrates by Nishino et al. (42) using a growth rate of 0.1 μm/min. at 1300°C. A slower growth rate of 0.05 μm/min. at 1360°C has been employed by the same group (29) to grow β-SiC films on (111) and (100) Si presputtered SiC intermediate layer. Substrates containing a single crystal β-SiC to a thickness of 4 μm can be obtained if a polycrystalline SiC buffer layer having a thickness less than 1000 Å was presputtered on the Si substrate temperature at 800°-1000°C. The highest growth rate of 0.3 μm/min. yet reported in the achievement of single crystal β-SiC films has been employed by Jackson and Howard (41) at 100 C.

It should be noted that the H_2 etching rate of the growing β-SiC layer on the SiC substrate becomes appreciable when the growth temperature is greater than 1550°C (38). Therefore, the true growth rate will be the deposition rate minus the etching rate at these elevated temperatures.

Berman et al. (38) have grown β-SiC thin films on α-SiC substrates at 900°-1700°C and subsequently annealed them at 1600°-2000°C. They have demonstrated that it is possible to improve the crystalline structure of the deposited layer by thermal annealing. However, continued annealing at 2000°C caused deterioration of the surface because of the evaporation of the Si.

A two-step process technique (i.e., chemical conversion followed by regular CVD) has been investigated by Kuroiwa and Sugeno (47). They prepared a thin layer of β-SiC on Si(111) substrates by chemical conversion of CH_4 or CCl_4 at 1300°C. Near and at the interface, this initial film was polycrystalline. However, the crystal structure near and at the surface of the film was single crystalline. This final structure was the subsequent CVD of β-SiC at 1300°-1360°C did not give a single crystal layer on top of the as-formed β-SiC substrate. Their problem may arise from the use of the gas combination of $SiCl_4$ and CCl_4, because still higher growth temperatures are required for these more stable gases. Furthermore their growth temperature is limited by the melting temperature of Si.

Most recently Matsunami and Nishino (48) have successfully employed the two-step process technique to grow β-SiC single crystal thin films on (100), (110) and (111) planes of Si substrates. The chemical conversion step was carried out using C_3H_8 either in a 10^{-2} Torr vacuum or in a regular CVD system using a H_2 carrier gas and 1 atm total pressure. The chemically converted β-SiC layer had a definite effect on the crystallinity of the subsequent CVD grown β-SiC layer. The optimum conditions for the conversion process at low pressures were found to be a C_3H_8 partial pressure of 10^{-2} Torr at 1200°C and a 4 min. conversion time for Si(111) substrates or a 6 min. conversion time for Si(100) substrates. The final optimum thickness of the vacuum converted β-SiC layer was 600-800 Å. The optimum conditions for the conversion in a 1 atm CVD system were found to be 1350°C in a H_2 flow of 1000 cc/min. for a conversion time of 2 min. with i) a 1.2 - 1.5 cc/min. C_3H_8 flow rate for Si(111) substrates, ii) a 0.8 cc/min. C_3H_8

film rate for Si(100) substrates, and iii) a 1.5 cc/min. C_3H_8 flow rate for Si(110) substrates. The final optimum thickness of the CVD converted β-SiC layer was about 200 Å. It is interesting to note that these optimum thickness values are less than 1000 Å which was the maximum thickness reported by most people wherein a single crystal β-SiC thin film could be obtained on a Si substrate by chemical conversion. Therefore, the subsequent CVD process is homoepitaxial growth which can be achieved at a slightly lower temperature than in the heteroepitaxial case. For example, single crystal β-SiC layers up to 20 μm can be grown reproducibly on converted Si(111) substrates at a temperature as low as 1230°C by using SiH_4 and C_3H_8 (Si/C = 1) mixed with H_2 at 1 atm (48). Epitaxial growth of β-SiC on converted Si(100) substrates can be obtained at 1300°C and above. The crystallinity of the β-SiC films on three different substrate orientations was found to be in the following order (111) (100) (110).

Both a single-step (direct CVD) process and a two-step (chemical conversion followed by CVD) process were employed in this research. The experimental aspects are presented in section III.

3. Formation of Silicon Carbide by Sputtering Processes

Sputtering of SiC (49) reactive sputtering (50b, 51) or evaporation of Si (50b, 52) in methane or acetylene have been successfully used in the Si substrate temperature range of room temperature (49) to 500-1200°C to also produce intermediate "substrates" of SiC which can serve as a more closely matched surface for the subsequent chemical vapor deposition of β-SiC thin films. Berman, et al. (49) using r-f sputtering of α-SiC onto the (100) plane of Si at room temperature was the first group to produce amorphous SiC which, if annealed at 1250°C-30 minutes, resulted in single crystal β-SiC. The thickness of the layer was approximately 1000 Å. Unfortunately this research was discontinued (along with the other SiC projects at AFCRL) before it could be tested as a substrate for the growth of thicker films by, e.g., CVD methods or additional sputtering. Nishino, et al. (53) have repeated the work of Berman, et al. but with the addition of the CVD growth step.

The amorphous deposit crystallized into a polycrystalline layer upon heating to the 1350°C - CVD temperature; however, it appeared to serve as a stress buffer between the Si and the subsequent thin film, as the latter grew as a single crystal. Unfortunately, the vacuum achieved prior to sputtering and the purity of the Ar used to sputter the SiC target were such that unacceptable levels of O and N were introduced into the growing film (as observed by Auger/SIMS analysis). These impurities were later introduced into the growing CVD films by auto-doping. These authors have also terminated this vector of their research.

The author of this proposal has redesigned and retrofitted a used r-f unit into a modern day system having the capabilities of digital and separate control of gas flow and pressure, a changeable target - substrate distance and a novel substrate heater. The experimental aspects of this research are also presented in Section III.

III. Experimental Procedures

A. CVD System Design for β-SiC Deposition

The variable pressure CVD apparatus constructed in-house and used to grow the β-SiC thin films in this research program is shown schematically in Fig. III-1. A brief explanation of the various lettered components is given on the succeeding page.

A total of seven different gases were used in the system in the complete experimental program. The principle reactant gases included silane (SiH_4) as the Si source and either methane (CH_4) or ethylene (C_2H_4) as the C sources. These were entrained in a carrier gas of either H_2 or Ar. The gaseous HCl was used to provide *in-situ* gas-phase etching prior to the deposition. Argon was also used to purge the system and to maintain the system in a hold condition during in-operation. The exhaust line was purged with N_2 to prevent the pyrophoric reaction of SiH_4 (i.e., it spontaneously ignites when in contact with air or H_2O). The impurity contents and vendors for each of these gases are given in Table III-1.

The high purity commercial H_2 was subjected to additional "in-house" purification using a Pd/Ag cell (H_2-P)[*1] with the capacity of producing higher purity H_2 (less than 0.1 ppm total impurities) at a rate of 5ℓ/min. An Ar purge capability for the pure H_2 delivery line allowed not only the purge action but also the ability to use Ar as a carrier gas. A line regulator (LR) was installed at the downstream side of the H_2 purifier to maintain a constant delivery pressure of pure H_2. A check valve (C) and a rotameter (R) were installed on the bleed line of the H_2 purifier to ensure a small unidirectional flow of the bleed gas.

[*1] Lettered symbols noted in parenthesis throughout the remainder of this report correspond to parts of the CVD system shown in Fig. III-2.

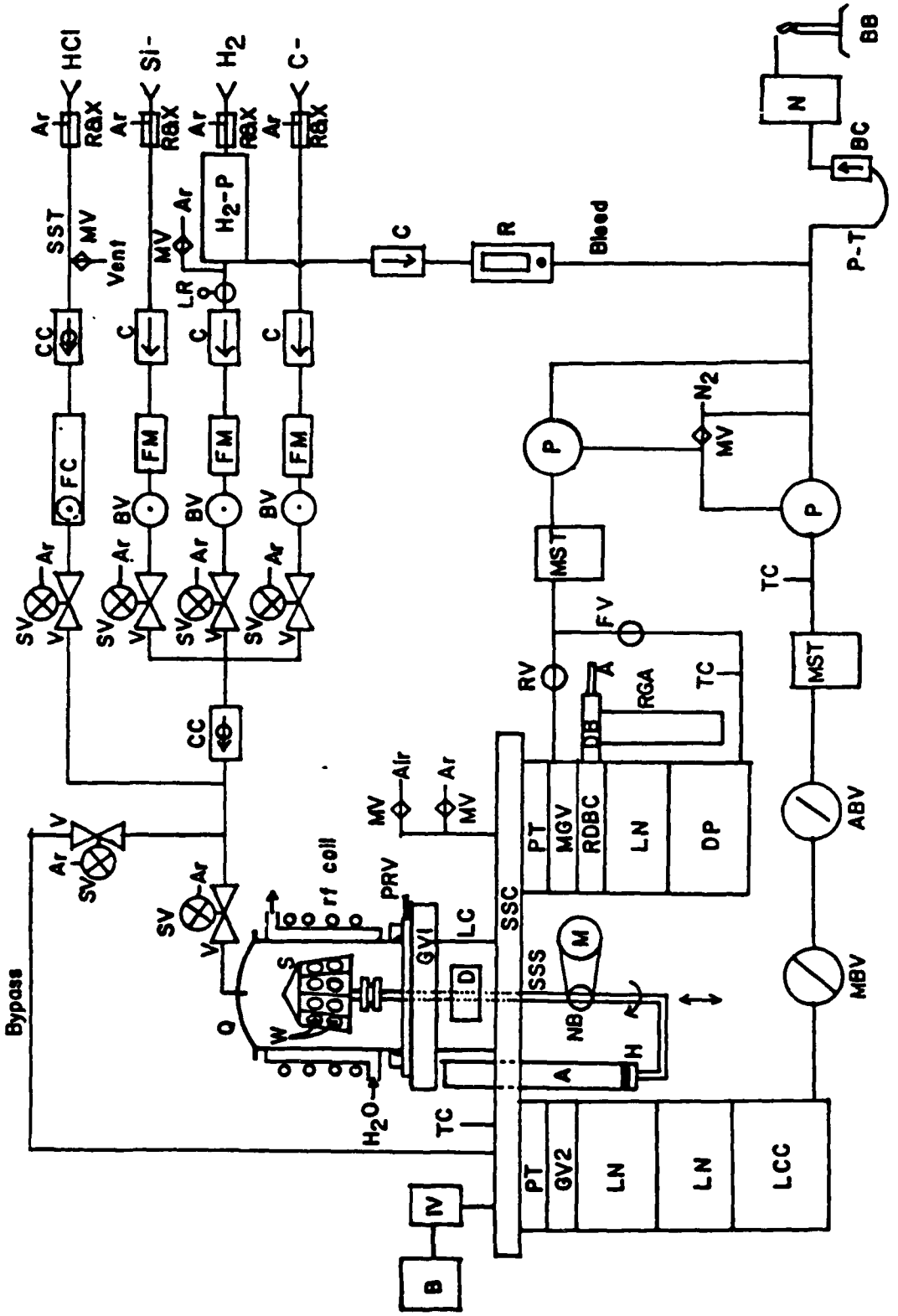

Figure III-1. Schematic representation of the variable pressure CVD apparatus constructed for the thin film growth of β-SiC. An explanation of the lettered components is given on the following pages.

Explanation of Lettered Symbols in Fig. III-1.

A = Air cylinder
ABV = Auto Butterfly Valve
B = Baratron pressure sensor
BB = Bunsen Burner
BC = Ball type Check valve
BV = Brooks Valve
C = Check valve
CC = Corrosion resistant Check valve
D = Door for loading chamber
DB = Differential Box for RGA
DP = Diffusion Pump
FC = Flow Controller
FM = mass Flow Meter
FV = Foreline Valve
GV1 = auto Gate Valve #1
GV2 = auto Gate Valve #2
H = Height adjust mechanism
H_2-P = H_2 Purifier (Pd/Ag diffuser)
IV = Isolation Valve for Baratron
LC = Loading Chamber
LCC = Liquid Collection Chamber
LN = Liquid Nitrogen cold trap
LR = Line Regulator
M = Motor
MBV = Manual Butterfly Valve
MGV = Manual Gate Valve
MST = Molecular Sieve Trap
MV = Manual Valve
N = Neutralization chamber for HCl gas
NB = Needle Bearing
P = mechanical Pump
PRV = Pressure Relieve Valve
PT = Particle Trap
P-T = P-Trap
Q = Quartz reaction chamber
R = Rotameter
R&X = Regulator and cross purge assembly
RDBC = RGA Differential Box Chamber
RGA = Residual Gas Analyzer
RV = Roughing Valve
S = Susceptor
SSC = Stainless Steel Chamber
SSS = Stainless Steel Shaft
SST = Stainless Steel Tubing
SV = Solinoid Valve
TC = Thermocouple Gage
V = pneumatic Valve
W = Wafer

Table III-1. Purities, Impurity Contents and Vendors for Each Gas used in this Research

Gases	Grade	Purity	Impurity Contents (ppm)						
			N_2	O_2	THC[*5]	OHC[*6]	CO & CO_2	H_2O	H_2
H_2[*1]	Pre-purified	99.995%	20	5	5		2	8	
Ar[*1]	Research	99.9998%	1	0.5	0.5		0.5		1
HCl[*2]	Electronic	99.995%	20	3	2		2	2	
SiH_4[*2]	Epitaxial	99.999%	5	0.5	0.2			1	5
CH_4[*3]	Research	99.9995%	2	0.5		0.1		2	0.1
C_2H_4[*3]	Research	99.99%	3			65			
H_2[*4]	Ultra High Purity	99.998%	Data not supplied by vendor						

*1 Airco Industrial Gases, Research Triangle Park, North Carolina.
*2 Scientific Gas Products Inc., South Plainfield, New Jersey.
*3 MG Scientific Gases, Somerville, New Jersey.
*4 Air Products, Raleigh, North Carolina.
*5 THC - Total Hydrocarbons Content.
*6 OHC - Other Hydrocarbon Content.

Stainless steel cross purge assemblies (R&X) were employed between the gas tank and the regulator to eliminate impurity capture during gas tank exchange. Stainless steel tubing (SST), specially cleaned for chromatographic experiments, was used throughout the system except for the feed line and the bleed line for the H_2 purifier wherein Cu tubing was employed. Check valves (C or CC) were employed in each line to prevent contamination of the lines and gas bottles in the event of back pressure buildup near or in the chamber. Swagelok^R and ultra-torr^R fittings were used to ensure a leak-tight system.

The mass flow rate of the two reactant gases and the carrier gas was measured by a mass flow meter (FM) which returned a signal to a pressure/flow ratio controller. The feedback signal was compared to the electrical setpoint extablished by the operator, and any difference amplified to adjust the electronic control valve (BV). An independent mass flow controller (FC) containing a flow control valve was used for the HCl; since, 1) the operator may desire to vary the amount of etch gas used for the Si and SiC, respectively, and 2) the flow control unit could handle only three gases.

The total pressure of a system such as this may be controlled by controlling the total input gas flow while simultaneously maintaining the ratio of the gas flow rates. As such, the total flow of each gas is determined as a portion of the total flow by the setpoint for each flow channel in the controller. Unfortunately, pressure changes may occur for reasons which have little or nothing to do with the gas flow. For example, the pumping speed of the mechanical pump may change during a run which would, in turn, change the rate of gas flow. This would change the nucleation rate of the depositing film and measurably alter the electronic characteristics of this layer. In the system developed for this research, the pressure was also maintained constant by using an exhaust valve controller which compared the actual system pressure (measured by a Baratron^R capacitance manometer (B)) with the desired setpoint and controlled a stepper motor-powered exhaust valve (ABV) to vary the pumping speed. In this way the control of pressure and flow

were completely separate and resulted in stable gas reaction kinetics and the nucleation of the SiC on the substrate.

Pneumatic bellows-sealed valves (V) operated by Ar in this system, were employed as an insurance measure against the possible closure failure of the electronic flow control valves and to establish the initial flow conditions of all gases before they enter the main chamber. Three-way normally closed solenoid valves (SV) controlled the supply of Ar gas to each pneumatic valve.

Gases were first vented through the bypass line to the mechanically pumped side of the stainless steel chamber (SSC) located below the reactor. When set flow rates were established, the gas mixture was immediately switched into the reaction chamber in order to contact the already heated substrates.

The reaction chamber was composed of a water cooled, clear fused quartz tubing (Q) mounted on a water cooled stainless steel fitting (similar to an ultra-torr fitting). Gases entered the reaction chamber from the top via sealed quartz tubing with a series of holes around the diameter. The water cooling jacket was a separate quartz tubing attached to the quartz reaction chamber by two O-ring sealed copper fittings. Cooling water entering the cooling jacket wrapped itself around the tube and flowed upward because of the spiral path in the bottom fitting. In this way, a more uniform temperature distribution inside the reactor was obtained. Making the reaction chamber and the cooling jacket two separate tubes enhanced the ease of cleaning, by allowing the chamber to be independently removed.

Copper tubing having a 3/8 in. diameter and wrapped very closely outside the water jacket served as the induction coil. The 10 kHz motor-generator type induction unit has 15 kW rated output power.

The barrel type susceptor (S) was normally a multi-flat high purity graphite device supported by a high purity Poco graphite assembly (see Fig. III-2) and a stainless steel shaft (SSS). The specially designed graphite assembly was employed to reduce the amount of heat transfer to the stainless steel shaft. The stainless steel shaft was

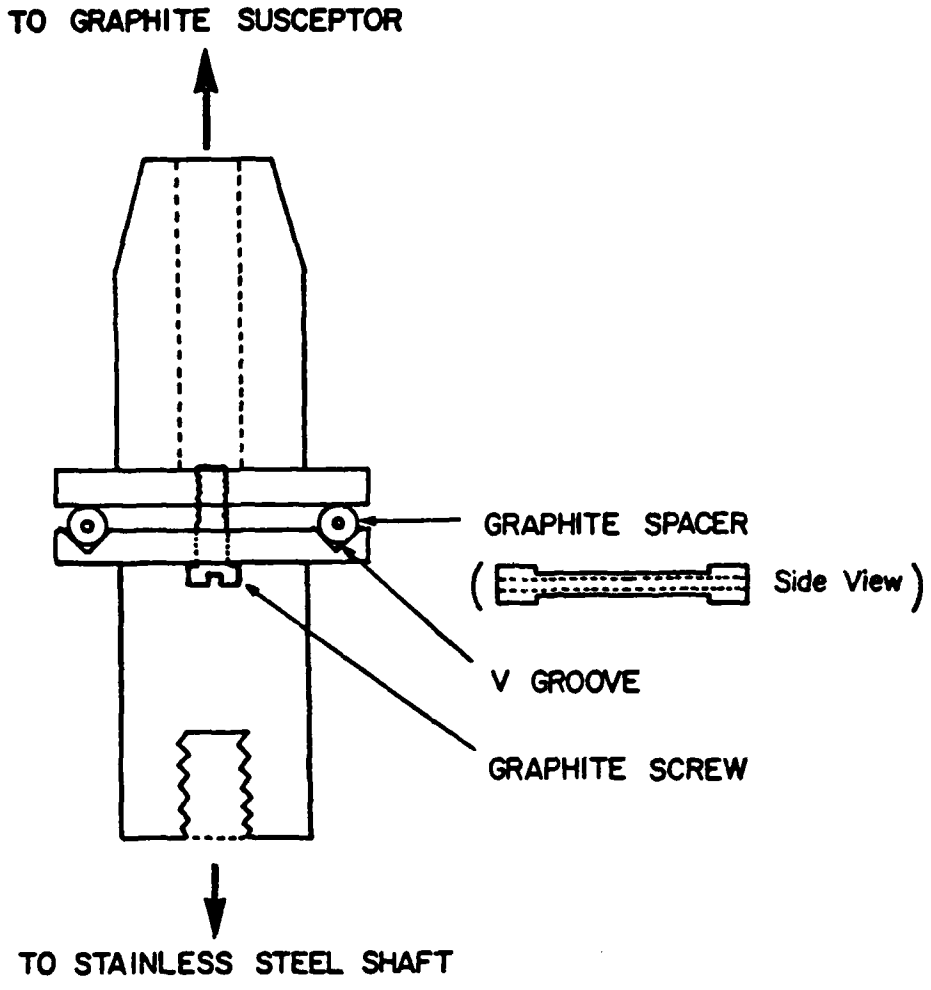

Figure III-2. Poco graphite assembly to connect the graphite susceptor to the stainless steel shaft.

attached to a hydraulic (A) and motorized (M & NB) assembly which allowed both rotation and vertical movement of the susceptor. Both motions allowed a change of samples in a loading chamber (LC) through an O-ring sealed door (D) without exposing the fused quartz chamber to air. Furthermore, the rotation of the susceptor during the deposition provided more uniform distribution of temperature as well as gas composition to each substrate. The vertical movement of the susceptor was interlocked with the gate valve (GV1) by microswitches and a solenoid valve to prevent any accidental damage. The susceptor's position relative to the gas inlet could be adjusted (H) by the stroke of the air cylinder. The maximum adjustment for that is 3 inches.

The cone-shaped top of the susceptor served two purposes: 1) it preheated the gas and helped the formation of the boundary layer, and 2) it gradually (rather than suddenly) reduced the cross sectional area between the susceptor and the inside wall of the chamber. A number of samples could be placed on the susceptor for each run.

Because the loading chamber was repeatedly exposed to the atmosphere, an isolation valve (IV) was installed for the Baratron^{R} to prevent any dust or moisture from depositing on the diaphragm. It was necessary to close this valve before venting the system to atmosphere.

A set of three gate valves was used to isolate the various parts of the reaction and pumping sections. Two of them (GV1 & GV2) were air-operated vacuum gate valves with a position indicator. The third one (MGV) was a manual gate valve with the roughing valve (RV) and the foreline valve (FV) built in. Particle traps (PT), which contained stainless steel filter media, were located above the gate valve for each pumping line. The diffusion-pumped side, including a residual gas analyzer (RGA), differential box chamber (RDBC) and a liquid nitrogen cold trap LN), were evacuated using a mechanical pump (P) and a diffusion pump (DP). This combination of pumps was also used to evacuate the total system and to differentially pump the RGA, which required a pressure below 5×10^{-4} Torr to operate. The other pumping assembly, including two liquid nitrogen cold traps, a manual butterfly

valve (MBV), an automatic exhaust control valve, and a mechanical pump, was used to maintain the gas flow during the actual run. The manual butterfly valve allowed a larger opening in the automatic valve for small amounts of gas flow and, therefore, closer control of the pressure. Molecular sieve traps (MST) were also included to prevent mechanical pump oil from backstreaming into the system. This trap can be regenerated by a built-in heater. If the trap becomes saturated with pump fluid, it becomes difficult to evacuate the system below 50 millitorr with the mechanical pump.

The loading chamber and the stainless steel chamber can be purged by Ar or vented by air through separate manual valves (MV). Three vacuum thermocouple gauge tubes (TC) were installed at proper locations for pressure measurement at one millitorr or higher. The pressures at the three locations were read on a thermocouple gauge meter.

The exhaust lines contained many special safety items, including N_2 purging arrangements for the space over the oil of the mechanical pumps, H_2 purge for the exhaust lines, sophisticated burn-off valving (BC) and trapping (P-T) devices to prevent backstreaming of air from entering the exhaust lines, and a box (N) constructed in-house and containing NaOH to neutralize any residual HCl before venting the various gases to the atmosphere. A combustible gas detector, with standard industrial type sensors located near the reaction chamber and on the ceiling of the laboratory, was installed to monitor any leakage of H_2 and/or hydrocarbon gases.

B. Procedures for Beta Silicon Carbide Thin Film Deposition

1. Susceptor Preparation

The barrel-type susceptors used in this research were made from a special graphite which had been purified in a Cl atmosphere at 2600°C after machining. The final impurity level was 10 ppm or less as measured by emission spectroscopy. The coefficient of thermal expansion of this graphite material matches very closely that of SiC. Therefore, it is particularly suitable as a susceptor material in semiconductor applications because a stable high purity and impervious

SiC may be deposited on it to prevent migration of impurities from the graphite to the substrate or the growing thin film. This coating was deposited *in-situ* in the CVD reactor described in the previous section.

2. Substrate Preparation

The commercially available single crystal Si wafers used in this research were both n-type and p-type with reported resistivities along the lengths of the two parent boules in the ranges of 37-420 Ω-cm and 10-50 Ω-cm, respectively. All wafers had a thickness of either 0.025" or 0.020" with $\pm$ 0.001" variation, and were 1° or 6° off-axis from the (100) plane and 2° or 4° off-axis from the (111) plane.

One side of the as-cut wafers was subjected to chemical-mechanical polishing using the Silver-Regh-Gardiner method. The polishing slurry consisted of cupric nitrate ($Cu(NO_3)_2 \cdot 3H_2O$) and ammonium fluoride (NH_4F) in water with no abrasive medium. The chemistry of this process involves a Cu replacement reaction in which Cu^{+2} ions are reduced to metallic Cu and Si is oxidized to Si^{+4}. The Cu is deposited on the Si wafer surface and may be wiped away with a polishing pad. Simultaneously, the oxidized Si reacts with the F^- ions and goes into solution as a fluorosilicate (SiF_6^{-2}). This process continues as new layers of Si are exposed. Normally, a half hour of polishing at room temperature removes about 0.005" of Si and results in a damage free surface. This procedure was followed by a multi-step cleaning process which rendered the wafer suitable for SiC deposition.

3. Deposition

An effective and successful technique which has been employed in this research to produce thin films of β-SiC involves the chemical conversion of the Si substrate surface as the initial step. This is followed by a CVD process for the growth of epitaxial β-SiC thin films. A schematic diagram for this two-step technique is illustrated in Fig. III-3. In this process the operational pressure during conversion and deposition was maintained constant at 760 Torr. A small amount (about 0.03v/o) of C_2H_4 gas mixed with the H_2 carrier gas was introduced

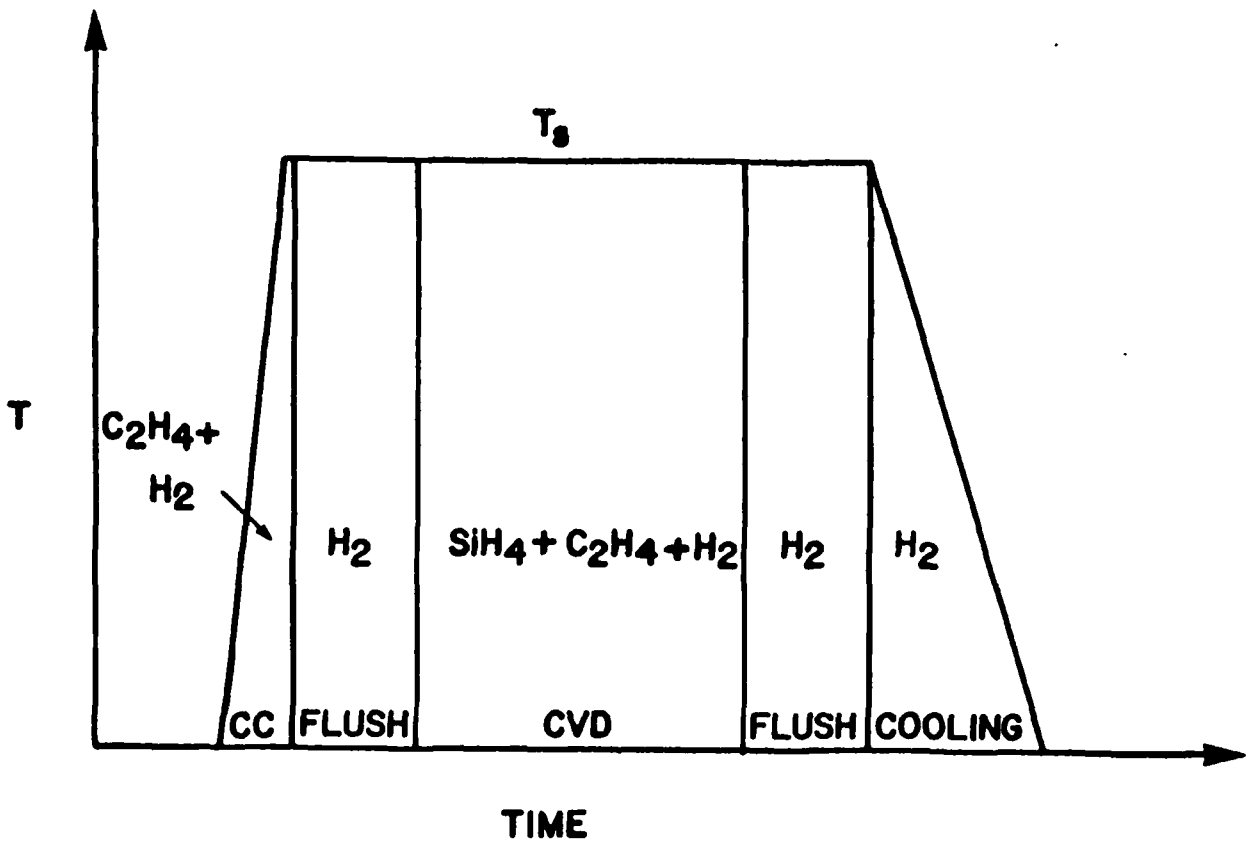

Figure III-3. A schematic diagram for the process of chemical conversion (CC) of the Si(100) or Si(111) substrate surface followed by the CVD process to grow epitaxial β-SiC thin films. Ts = substrate temperature.

into the reaction chamber prior to the heating process. The substrates were heated as quickly as possible from room temperature to the conversion temperature. The total conversion time was only 2-3 minutes. After chemical conversion, the reaction chamber was flushed by H_2 for about 5-10 minutes. A common CVD process was followed; therefore, it was necessary to explore a large number of deposition temperatures, rates of heating and cooling, reactant partial pressures, total pressures, and flow rates in order to determine the most suitable scenario for β-SiC deposition. These final parameters are reported in the Results and Discussion Section.

C. Characterization of CVD Beta Silicon Carbide Thin Films

1. *Surface and Thickness Evaluation*

Both optical and scanning electron microscopy were employed to examine the as-grown surface and to measure the thickness of the β-SiC films. The latter instrument was used on a routine basis as it offered superior resolution and depth of field.

The SEM samples were mounted on an Al stud using an electrically conductive carbon paint (colloidal graphite in isopropanol). Electron charging was not a problem because the β-SiC films were found to be sufficiently conductive; thus, no conductive coating on the film was necessary. Staining was also not necessary as the contrast between the β-SiC film and the Si substrate was very good. The SEM samples in the chamber were tilted at a 45 degree angle to the incident electron beam unless noted otherwise in this report.

2. Structure Characterization

To determine the single or polycrystallinity of the β-SiC films grown by the CVD technique in the research, both X-ray and selected area electron diffraction techniques were conducted. The basic differences between these two techniques are the wavelength of the diffracted radiation and the diffracted intensity. The x-ray technique provides information concerning the structure within the volume of the thin film, while electron diffraction provides the crystal structure only

close to the film surface or within certain layers of the thin film, depending on the angle of diffraction.

a. X-ray Techniques

Pole figure determinations and the Laue method were employed in this research to examine the crystal structure of the β-SiC thin films.

A reflection type pole figure device (Schulz goniometer) was employed to check the single or polycrystallinity and the epitaxial relationships of the grown film. Figure III-4 shows the schematic diagram for the reflection type pole figure arrangement. This equipment uses a special sample holder which allows rotation of the specimen either in its own plane about an axis normal to its surface (the sample axis (AA')) or about a horizontal axis (the goniometer axis (BB')). Complete 360° rotation is permitted about the AA' axis, while up to $\pm$ 70° about the BB' axis is allowed on the goniometer.

The BB' axis which is in line with the incoming x-ray beam is initially set at an angle which is the approximate angle that the Si wafers deviate from the true (111) or (100) surface. This setting makes equal angles with the incident and diffracted beams. The initial Bragg angle for the Si substrate is set at about the x-ray equipment axis (CC'). Each sample is slowly rotated about the sample axis AA' until diffraction conditions for Si occur. One must adjust the AA', BB' and CC' axes individually to obtain the strongest signal and then record that peak on a chart. Once the sample is oriented for Si diffraction, the AA' and the BB' axes are fixed and the Bragg angle is subsequently changed to be very close to that for the diffraction condition of the β-SiC plane which is parallel to the surface plane of Si. The goniometer is then automatically scanned about the CC' axis for a few degrees in order to cover the Bragg angle of the expected β-SiC diffraction plane. The result of this scanning procedure is recorded simultaneously. If the epitaxial growth of β-SiC has been obtained on the Si substrate, a peak will be observed on the chart. In addition, a 1°/28/min. x-ray scan of the β-SiC film on the Si

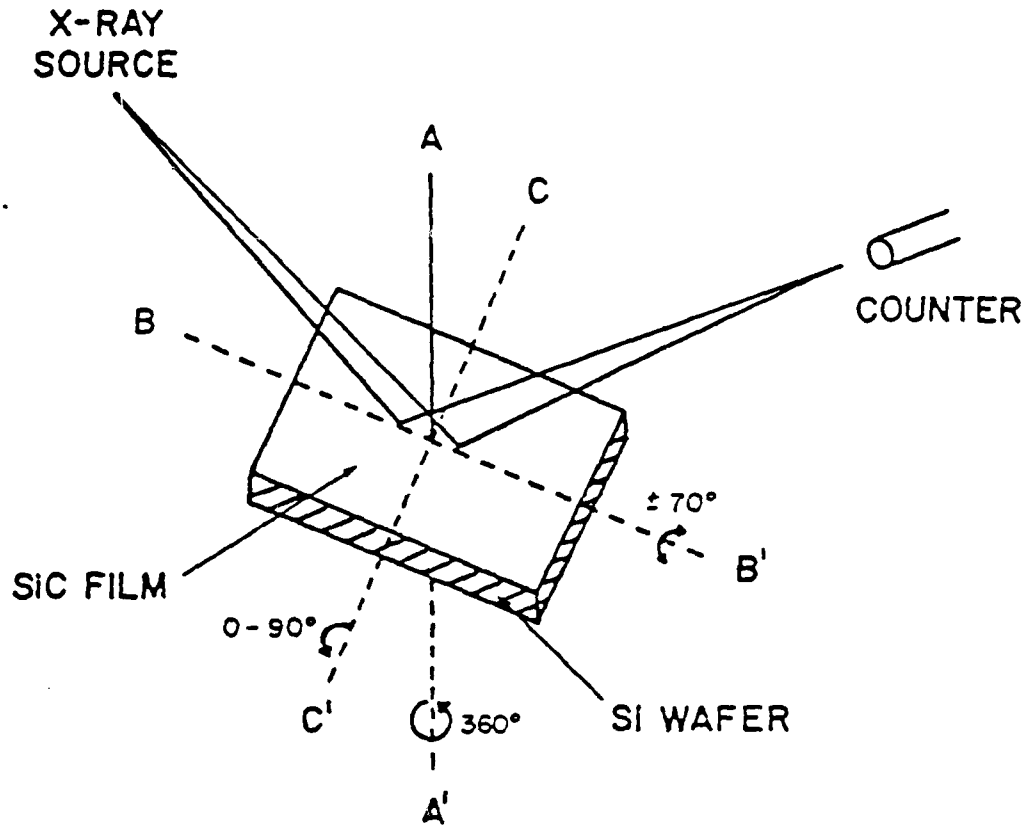

Figure III-4. Schematic diagram for a x-ray reflection type pole figure examination of the SiC thin film.

substrate from 77° to 25° is used to reveal the absence of any extra peaks which may be caused by the diffraction of polycrystalline layers or a second phase.

CVD structures may also grow in a fibrous manner wherein the film is formed from successively deposited layers which are polycrystalline in nature or result in single crystal fibers or pyramids. If the fiberous structure exists but the individual fibers are oriented randomly in relation to one another, one may indirectly discern their presence by rotating the aforementioned sample about the BB' axis at an angle corresponding to the interplanar angle between the surface plane and another plane of the diamond cubic structure. For example, 35° between the (111) and (220) planes, and 45° between the (100) and (220) planes. The Bragg angle is now changed to read the new Si peak and subsequently changed again to record the β-SiC peak. If the fibers are oriented randomly with respect to each other, no change in the measured intensity of the diffracted beam will be observed and polycrystallinity may be assumed. If the fibers are oriented in the same way relative to each other (some people consider this to be a single crystal), or if the film is actually a single crystal (one grain crystal), three peaks will be found at 120° from each other for the β-SiC film grown on a Si(111) substrate; since, the (111) orientation has 3-fold symmetry. Four peaks will be found at 90° from each other for the β-SiC film grown on a Si(100) substrate; since, the (100) orientation has 4-fold symmetry. In this case poly- and single crystallinity cannot be differentiated and must be discerned by microscopy techniques.

A Laue photograph is one of the easiest diffraction patterns to produce, and it was used extensively in this research program. In the Laue method, the Bragg equation, $n\lambda=2d\sin\theta$, is satisfied by effectively varying the wavelength λ using a beam of continuous (white) radiation.

Since Laue spots from the same crystallographic family of planes are superimposed and independent of the interplanar spacing, two crystals of the same orientation and crystal structure, but having different lattice parameters will produce identical Laue patterns.

Because β-SiC and Si are both diamond cubic structures the Laue pattern for both of them will be exactly the same, assuming epitaxial growth occurred. It is necessary, therefore, to examine the β-SiC film alone in order to eliminate the effect from the Si substrate. The transmission Laue samples were prepared by waxing the whole sample except a 2 mm central spot in the back of the Si substrate, immersing the sample in an $HF+HNO_3$ (2:3 ratio) mixture to etch a hole on the Si, rinsing in deionized water and dissolving the wax in trichloroethylene. The remaining Si substrate acts as a support for the SiC film.

If the grown film is polycrystalline and randomly oriented in character, complete Debye rings will appear on the film. If the grown film has layers of both single crystal and polycrystalline material, the resulting patterns will have superimposed Laue spots and Deybe rings. Therefore, the advantage of the transmission Laue technique is that the volume structure of the thin film can be obtained.

In a transmission Laue pattern, the spots are all elliptical with their minor axes aligned in a radial direction. Furthermore, spots near the center and edge of the pattern are thicker than those in the intermediate positions. The spots become distorted and smeared out if the crystal has been bent or twisted in any way. Therefore, the Laue method also provides an assessment of crystal perfection.

It should be noted that, in practice, the symmetry pattern on a Laue photograph is very sensitive to the precise orientation of the crystal. Slight deviation from the ideal position will result in a distortion of the relative positions and intensities of the spots on the photographs. This may occur very easily, as the Si substrates used in this research are normally misoriented a few degrees from the major axis.

Another particular problem is caused by the presence of characteristic radiation, when the unfiltered beams from diffraction tubes formerly used for powder diffraction studies are used for Laue work. If a set of planes happens to diffract this radiation, the resultant image would be exceptionally strong, and its intensity can not be compared with those of other spots.

b. Electron Diffraction

Electron diffraction methods are also frequently applied to the study of thin films. The symmetry and the spatial distribution of the diffraction spots or the diffraction rings may be used to determine the orientation and crystal structure of the specimen. Two common methods employed in this research were transmission electron diffraction (TED) and reflection electron diffraction (RED).

Transmission electron diffraction is restricted to specimens of thickness smaller than the penetrating depth of the fast electrons employed. The thickness limit is generally of the order of 2000 Å or so depending on the energy of the electrons. To prepare such a thin sample for TED work, the ion beam thinning technique was employed. The sample was first mounted on a glass plate using black wax with the β-SiC film against the glass plate, and then cut to a smaller size of 3 mm diameter using an ultrasonic impact grinder. After demounting and cleaning, the sample was mounted again on a thick pyrex glass disk with the β-SiC film against the glass and mechanically polished to about 3μ thick through grit 400 and 600 emery papers as well as 0.3μ and 0.5μ alumina solutions. An ion mill was used to thin the sample from the Si substrate side at an angle of 15° to the surface.

Reflection diffraction of high energy electrons occurs by penetration of a thin surface layer with ensuing diffraction and by transmission through surface protrusions of the film material. If the surface is reasonably rough, the beam can penetrate the asperities and the system is basically the same as TED. However, if the surface is atomically quite smooth, at shallow angles, penetration is quite low and the diffraction will respond to essentially the first few surface layers. Furthermore, surface contamination and oxide layers show up markedly on the reflected patterns, and the background of the inelastically reflected electrons is generally higher than in transmission patterns. Therefore, RED is very sensitive to surface conditions but less accurate than TED. However, the big advantage of using RED is

that the film can remain on the substrate which eliminates tedious sample preparation.

3. Electrical Properties

The Van der Pauw technique was used to measure the electrical properties of the as grown β-SiC films following the ASTM Standard Method F-76-68. These measurements consisted of the basic Hall data which gave the resistivity (P) and the Hall coefficient (R_H) from which the Hall mobility (μ_H) as well as the carrier type and concentration could be calculated.

In order to use the Van der Pauw technique, the epitaxial layer must be on a control substrate having either high resistivity or opposite electronic type. To meet this requirement, both n-type and p-type Si substrates were employed in this research because both p- and n-type SiC resulted from the CVD experiments.

Another requirement for the Van der Pauw method is that the electrical contacts must be ohmic in nature. Possible ohmic contact materials for n-type SiC films are Ni, Ag, Ti and a Ta-Au alloy among which the most reliable and the most widely used is Ni. Conductive Ag paste and In were tried without success in this research as the contact material for n-type β-SiC thin films.

To obtain a good ohmic contact on n-type β-SiC films, an electron-beam evaporated Ni film with a thickness of 2000 Å was initially deposited on four corners of a 5mm x 5mm square sample. This process was achieved by using an Al mask with holes at the appropriate corner positions. The sample was then sintered at 1100°C for 5 min. in vacuum. The I-V characteristic of the Ni contact is shown in Fig. III-5 and reveals the ohmic nature of this contact.

D. R-F Sputtering Facility

Another major effort in this program has been the design of an adjustable target r-f sputtering unit with separately controlled gas input and pressure regulation around the pumping system, 2.5 kv power

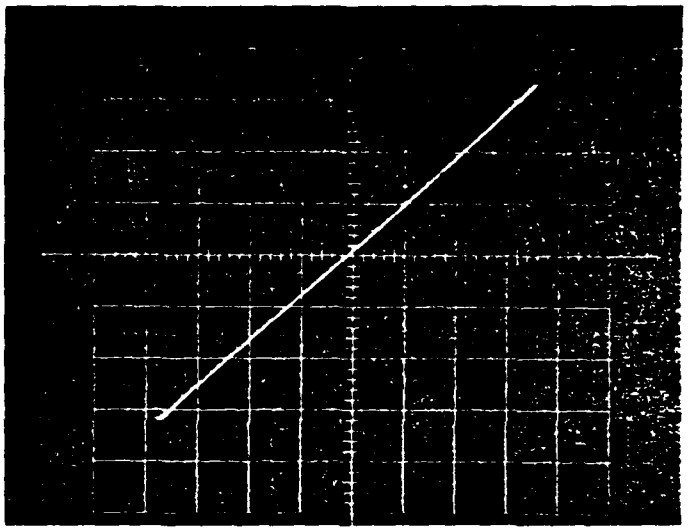

Figure III-5. I-V characteristic showing ohmic contact of Ni on an n-type β-SiC thin film. Vertical axis = 0.5 $MA/_{Div}$; Horizontal axis = 0.5 $V/_{Div}$.

supply and tuning networks of an older commercial unit. As in the case of our chemical vapor deposition unit, we have chosen to independently control both the flow rate of the entry gas (or gases, if reactive sputtering is employed) and pressure with the use of mass flow transducers and an automatically controlled servo-mechanical valve, respectively. The valve is actuated in response to a difference between the desired setpoint pressure and that determined by a capacitance manometer. The reason for this arrangement is to avoid fluctuations in the sputtering rate and therefore the necleation rate of the growing film which can easily lead to the growth of a polycrystalline film.

We have also designed a special β-SiC target which has been grown by chemical vapor deposition by Deposits and Composites Corporation of Reston, Virginia. This target is considerably superior in purity and density to that of any other type of commercial α or β-SiC.

Members of the SiC thin film group have also designed and implemented a special substrate heater which employs three 500 w quartz lamps. This heater has been used both as an anode to bias the plasma and etch the substrates.

IV. Results and Discussion

A. Si-C CVD Phase Diagrams

The results of this portion of this research program are presented as CVD phase fields as a function of temperature and Si/Si+C ratio in the input gas. The system pressure and the concentration of the carrier gas (e.g., H_2 or Ar) are varied systematically. The CVD phase diagrams presented here should not be confused with traditional composition-temperature phase diagrams. In most of the CVD diagrams the abscissa is the Si/Si+C ratio in the input gas, which does not fix the Si/Si+C ratio of the condensed phases. The "single phase fields" referred to in this work are conditions for which condensed species are deposited alone, without codeposition of any other species. Because of the considerable interest in CVD at 1 atmosphere as well as higher pressures (HPCVD) and lower pressures (LPCVD), a fairly wide range of total pressures have been considered in this research.

In the case of the CH_3SiCl_3/H_2 and $(CH_3)_2SiCl_2/H_2$ systems, the Si/Si+C ratios of the input gas are fixed. As such, the resulting phase fields are presented as a function of temperature and H_2/CH_3SiCl_3 or $H_2/(CH_3)_2SiCl_2$ mole ratios.

In preliminary calculations of the CVD phase diagrams, many minor species were included. Subsequent calculations omitted species of very low concentration ($< 10^{-18}$ mole percent) in order to minimize computing time. It has been shown that these do not effect the CVD phase diagrams.

The necessary thermodynamic values for most of the species were taken from the JANAF tables(54). The data for argon was taken from Ref. (55). Note that the JANAF tables give β-SiC a lower free energy than the α-form at all temperatures. No α-SiC was therefore predicted to occur under the conditions considered in the present work. The literature does not give clear experimental evidence to support or to contradict this result (56-59). The tables also give graphite as the stable condensed form of C and is accordingly the only form considered in this research.

(1) The $SiH_4/CH_4/H_2$ System

The species considered in this and the following two systems are gaseous H, H_2, SiH_4, SiH, Si, CH_4, C_2H_4, CH_3, C_2H and C_2H_2. The condensed phases considered are β-SiC, α-SiC, Si(s), Si(ℓ) and C(s) (graphite). The conditions include Si/Si+C mole ratios from 0 to 1, $H_2/(SiH_4+CH_4)$ mole ratios from 0 to 1000, and pressures from 10 atmospheres to 10^{-3} atmospheres.*

The calculated CVD phase diagrams for this system are shown in Figs. IV-1-4. It is immediately clear that the magnitude and position of the β-SiC single phase fields are sensitive to all the above parameters. While β-SiC is deposited under almost all conditions, codeposition of a condensed carbon or silicon phase is the dominant feature. At the highest system pressure of 10 atm., the single phase β-SiC field is small at low H_2 carrier gas concentrations, but increases markedly as the concentration of this gas increases (see Figs. IV-1(a)-1(d). The system behaves in a similar fashion at 1 atm. total pressure (Figs. IV-2(a)-2(d).

At a system pressure of 0.1 atm., the necessity for high H_2 carrier gas concentrations becomes very apparent as shown in Fig. IV-3. For $H_2/(SiH_4+CH_4)$ ratios from 0-50 (Figs. IV-3(a)-(c)), the β-SiC single phase fields are found only when Si/Si+C ≈ 0.5. Both high temperature and low temperature single phase fields occur at $H_2/(SiH_4+CH_4)$ ratios of 10 and 50. As the H_2 carrier gas concentration is further increased, the two β-SiC fields enlarge and join (Fig. IV-3(d), but remain located primarily at Si/Si+C < 0.5.

The necessity for high H_2 carrier gas concentrations is again apparent when the total system pressure is 10^{-3} atm., as shown in Fig. IV-4. However, in this case the β-SiC single phase field is

---

*The unit of pressure most commonly reported in the prior literature on the CVD of SiC has been the atmosphere. This unit has also been chosen for the present research in order to facilitate comparison of results with those previously reported by other investigators. The conversion factors to other units include: 1 atm. = 0.1013MPa = 760 Torr.

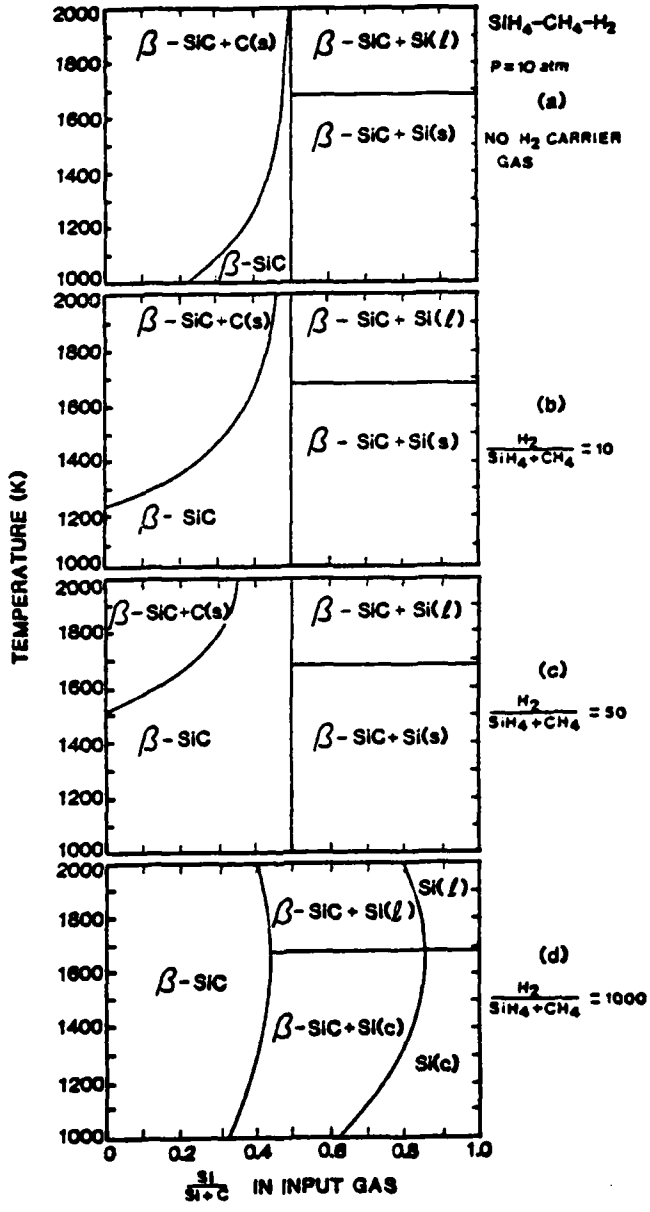

Figure IV-1. The $SiH_4/CH_4/H_2$ system at 10 atm. (1.013×10^6Pa) total pressure and various H_2 carrier gas concentrations.

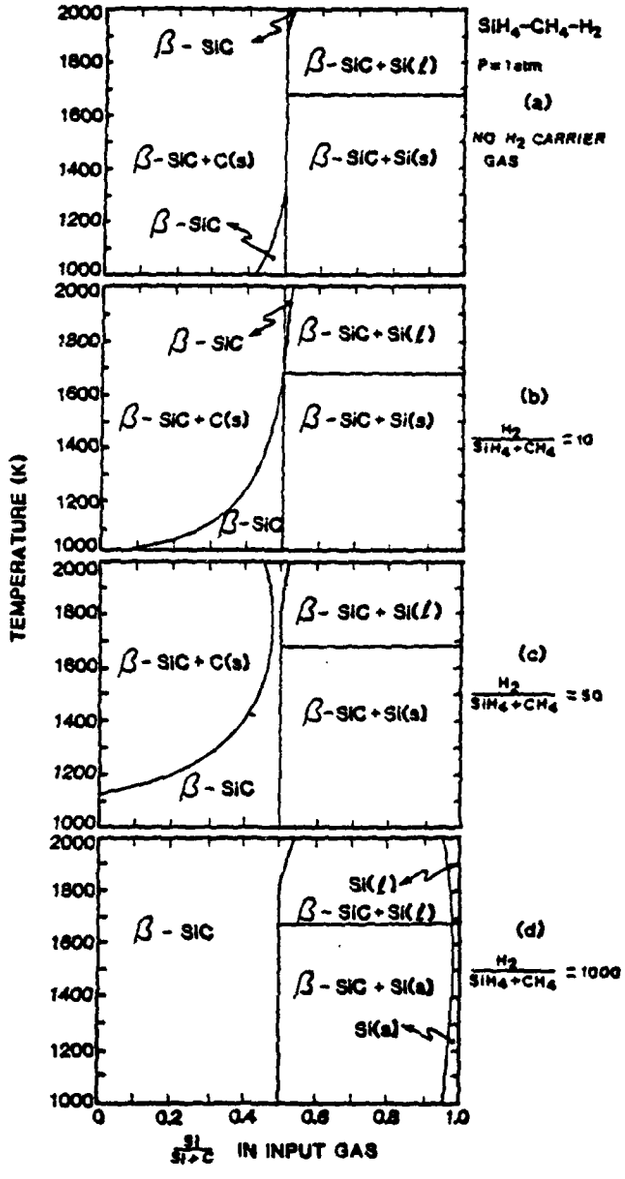

Figure IV-2. The $SiH_4/Ch_4/H_2$ system at 1 atm. (1.013×10^5Pa) total pressure and various H_2 carrier gas concentrations.

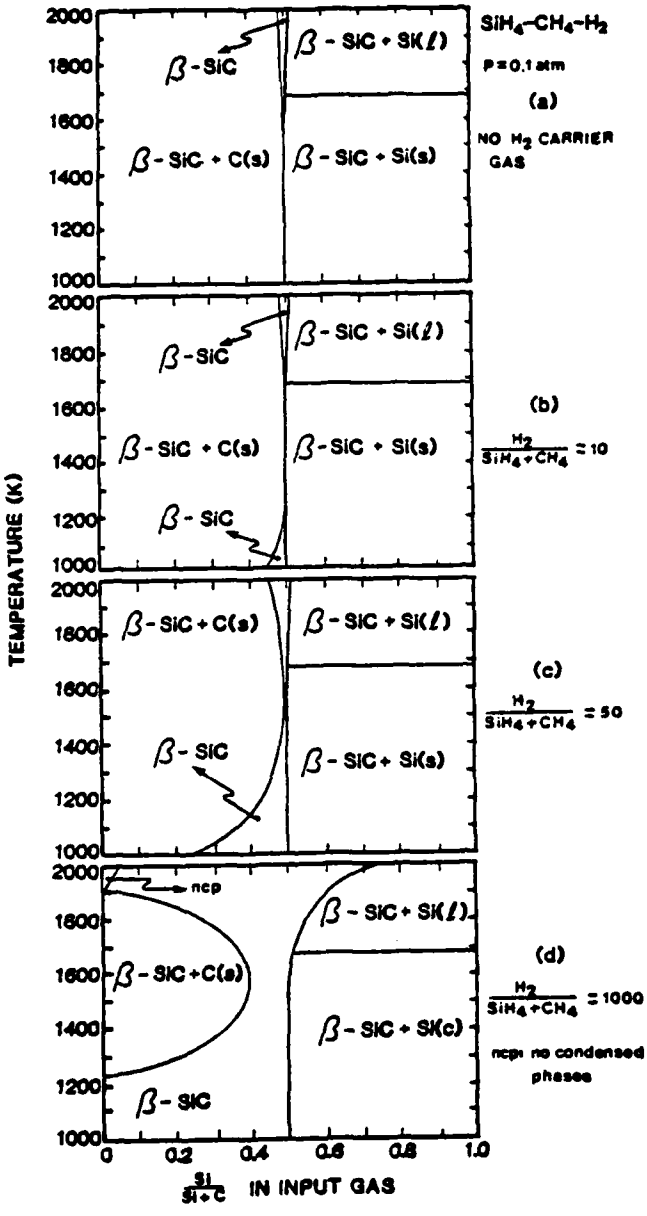

Figure IV-3. The $SiH_4/CH_4/H_2$ system at 0.1 atm. (1.013×10^4Pa) total pressure and various H_2 carrier gas concentrations.

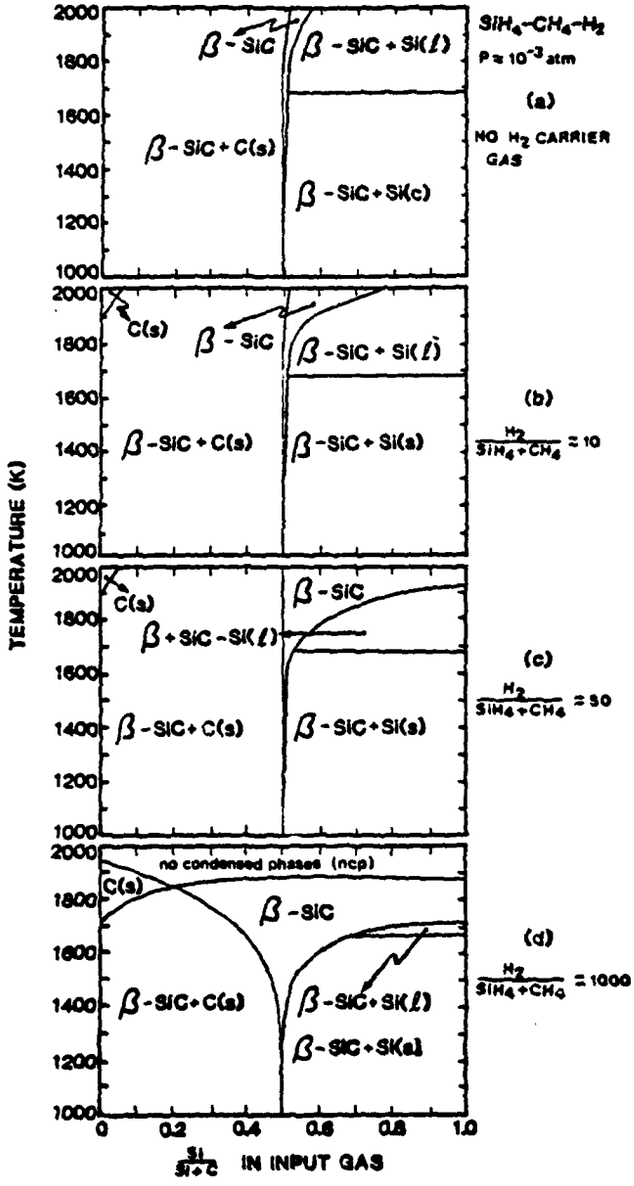

Figure IV-4. The $SiH_4/Ch_4/H_2$ system at 10^{-3} atm. (1.013×10^2Pa) total pressure and various H_2 carrier gas concentrations.

located only at the higher temperatures, and predominantly at higher silane concentrations than described previously, i.e. at Si/Si+C > 0.5 (Figs. IV-4(c) and (d)).

The CVD processor is normally limited in the pressure at which he can operate by the equipment at his disposal. If operating under equilibrium conditions at 1 atmosphere, the above results indicate that the H_2 concentration should be relatively high, and the Si/Si+C ratio in the input gas approximately 0.4 in order to maximize deposition efficiency and minimize the codeposition of Si or C. If it is desired to operate the system at low pressures of $\approx 10^{-3}$ atm. (LPCVD), then the above results suggest that one should operate at higher temperatures as well as higher SiH_4 and H_2 concentrations.

At low temperatures (~1000K), the calculated equilibrium composition of the gas phase is simple, as shown in Table 1, with H_2 the species of highest concentration, even at zero carrier gas concentrations. The predominant C-Containing species in the gas phase is CH_4. At Si/Si+C ratios ~ 0.5, the concentrations (and partial pressures) of the Si-containing species are lower, with SiH_4 of greatest significance. The concentrations of CH_4 and SiH_4 are directly dependent on the total system pressure, as shown in Table IV-I and discussed below.

At higher temperatures (>1500K) the gas phase composition becomes substantially more complex as concentrations of species such as Si(g), SiH, C_2H_2, C_2H and CH_3 become significant (Table IV-II). Again, total pressure affects the composition but in a more complex way than at the lower temperatures.

It should be noted that condensed phases with concentrations as low as 10^{-18} mole percent are included in the CVD phase diagrams. At $<10^{-18}$, the concentration of that phase is equated to zero. However, the concentrations of a condensed phase changes very sharply at the boundary of that phase. For example, setting the concentration of the phase equal to zero when it reaches 10^{-1} mole percent, results in only a very slight shift in the phase fields shown in the Figs., typically less than 0.02 units of Si/Si+C.

Table IV-I. SiH_4/CH_4 System: Equilibrium Gas Phase Composition at 1000K (Si/Si+C = 0.5)

Species	Species Partial Pressure (atm)	
	at P = 10 atm*	at P = 10^{-3} atm*
H	0.71×10^{-8}	0.71×10^{-10}
H_2	0.99×10^{1}	0.10×10^{-2}
SiH_4	0.63×10^{-4}	0.63×10^{-12}
CH_4	0.37×10^{-2}	0.38×10^{-10}
C_2H_4	0.90×10^{-11}	0.91×10^{-19}
CH_3	0.55×10^{-10}	0.55×10^{-16}
C_2H	$< 10^{-20}$	$< 10^{-20}$
C_2H_2	0.12×10^{-14}	0.21×10^{-18}
SiH	0.39×10^{-13}	0.39×10^{-15}
Si	0.16×10^{-15}	0.16×10^{-15}

*Total system pressure

Table IV-II. SiH_4/CH_4 System: Equilibrium gas Phase Composition at 2000K (Si/Si + C = 0.5).

Species	Species Partial Pressure (atm)	
	at P = 10 atm*	at P = 10^{-3} atm*
H	0.51×10^{-2}	0.50×10^{-4}
H_2	0.99×10^{1}	0.94×10^{-3}
SiH_4	0.18×10^{-3}	0.57×10^{-13}
CH_4	0.21×10^{-2}	0.35×10^{-9}
C_2H_4	0.16×10^{-5}	0.48×10^{-11}
CH_3	0.27×10^{-4}	0.45×10^{-9}
C_2H	0.16×10^{-7}	0.53×10^{-7}
C_2H_2	0.26×10^{-4}	0.83×10^{-6}
SiH	0.95×10^{-4}	0.50×10^{-7}
Si	0.42×10^{-4}	0.23×10^{-5}

*Total system pressure

It is of value to discuss the results shown in Figs. IV-1-4 in terms of simple equilibria. This allows one to explain the effect of H_2 and the total pressure. At lower temperatures (<1500K) it is useful to interpret the results in terms of the following competing equilibria:

$$SiH_4 + CH_4 \rightleftharpoons SiC + 4H_2 \qquad \text{equ. (1)}$$

$$CH_4 \rightleftharpoons C(s) + 2H_2 \qquad \text{equ. (2)}$$

$$SiH_4 \rightleftharpoons Si(s) + 2H_2 \qquad \text{equ. (3)}$$

Comparison with Table IV-I shows that these account for all important species.

The larger molar volume for the products in all these equilibria suggest that increasing pressure will shift the equilibria to the left. In a similar way, increasing the concentration of H_2 by introducing a carrier gas should have the same effect. In practice, both the CVD phase diagrams and the calculated equilibrium concentrations of the gaseous and condensed phases show that, while the overall equilibrium is shifted to the left, the individual equilibria are affected to different extents. For example, Figs. IV-1(a)-(d) show that as the H_2 concentration is increased, equilibrium (2) is driven to the left, without substantially affecting equilibrium (1), resulting in large single phase β-SiC fields as desired. Comparison of Figs. IV-3(b), IV-2(b) and IV-1(b) gives an example of increasing pressure working in the same way to increase the β-SiC single phase field.

The CVD phase diagrams show that this same method for increasing the β-SiC phase field cannot generally be applied when $Si/Si+C > 0.5$, and $P > 0.1$ atm. For example, comparison of Figs. IV-1(a)-(d) shows that in fact equilibrium (1) is shifted to the left rather than (3) as the H_2 carrier gas concentration is increased, resulting in condensed single phase Si rather than single phase SiC. The same occurs as total pressure is increased (see Figs. IV-3(d), IV-2(d) and IV-1(d)).

At temperatures > 1500K, SiH_4, CH_4 and H_2 do not totally represent the species present in the gas phase after equilibration. Other species, as noted previously, should be included in equilibria (1)-(3). However, the logic used to explain the occurrence of the single and binary phase fields in the preceding discussion remains the same. In the case where

$P \approx 10^{-3}$ atm, increasing the H_2 concentration does increase the size of the β-SiC field for Si/Si+C > 0.5 (Figs. IV-4(a)-(d)).

The effect of Ar on the CVD process is not nearly as marked as that of H_2. This is expected as Ar does not interact chemically to affect the equilibria. Comparison of Fig. IV-5 with Figs. IV-1(a)-(d) shows that the use of Ar as a carrier gas results in calculated CVD phase diagrams most similar to those where no H_2 is present. Comparison with Figs. IV-1(a) and IV-2(a) indicates that Ar has an effect similar to slightly lowering the total system pressure.

(2) The $SiH_4/C_2H_4/H_2$ System

This system is thermodynamically similar to the $SiH_4/CH_4/H_2$ system. The concentrations of the species in the gas phase after equilibration are almost identical to those determined in the previous system. Differences arise only from different H_2 concentrations (considering C_2H_4 as $C_2H_4/2$, and are therefore only expected to be significant at lower or zero H_2 carrier gas concentrations. This is confirmed in Fig. IV-6, which gives an example of the small shift of the β-SiC phase field when ethylene is used in place of methane.

(3) The $SiH_4/C_3H_8/H_2$ System

Once again, the equilibrium calculations predict the single phase fields to be similar to those of the CH_4 system, with the boundaries falling between those for the CH_4- and the C_2H_4-containing systems.

(4) The $SiCl_4/CCl_4/H_2$ System

The species considered to be in the gaseous phase of this system, and all the Si-C-Cl-H systems are: H, H_2, SiH_4, SiH, Si, CH_4, C_2H_4, CH_3, C_2H, C_2H_2, $SiCl_4$, $SiCl_3$, $HSiCl_3$, $SiCl_2$, SiH_2Cl_2, SiH_3Cl, SiCl, Cl, HCl, CH_3Cl, Cl_2, CCL and CCl_4. The condensed phase species considered are β-SiC, α-SiC, Si(ℓ), Si(s) and C(s) (graphite).

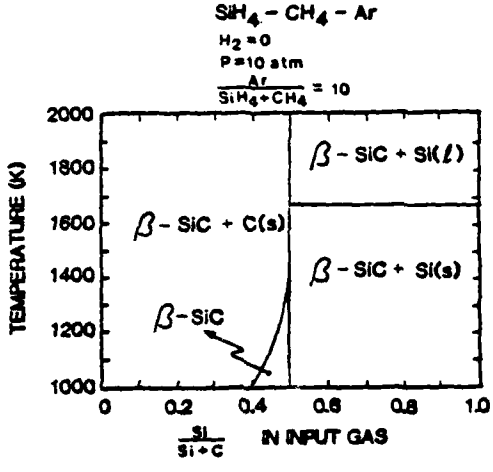

Figure IV-5. The SiH_4/CH_4 system with Ar carrier gas. Total pressure 10 atm (1.013×10^6Pa).

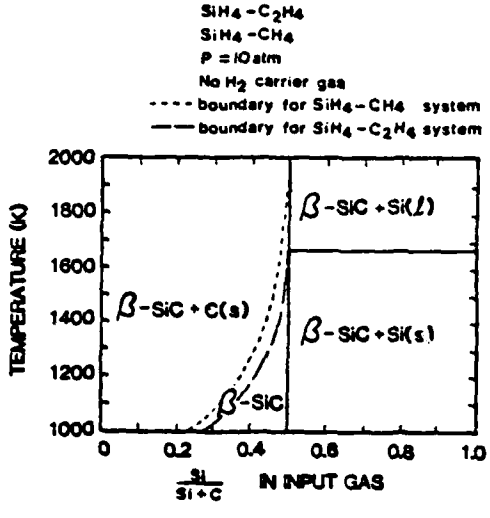

Figure IV-6. Comparison of the SiH_4/CH_4 and SiH_4/C_2H_4 systems at 10 atm (1.013×10^6Pa) and without carrier gas.

In the $SiCl_4/CCl_4$ system with no carrier gas, C is the only condensed phase formed under the conditions considered. By referring to the equilibrium concentrations of species in the gas phase (see Table IV-III for example) it is possible to describe the situation in terms of the following competing equilibria:

$$SiCl_4 + CCl_4 \rightleftarrows \beta\text{-}SiC + 4Cl_2 \qquad \text{equ. (4)}$$

$$CCl_4 \rightleftarrows C(s) + 2Cl_2 \qquad \text{equ. (5)}$$

$$SiCl_4 \rightleftarrows Si(s) + 2Cl_2 \qquad \text{equ. (6)}$$

For the conditions given, equilibrium (5) is the only one which is partly to the right. Thus graphite is the only phase deposited. It should be noted that at temperatures greater than 1200K, the concentration of the species Cl becomes significant in the vapor phase (Table IV-III); at 2000K the concentrations of Cl and Cl_2 are essentially equivalent. In addition, the species $SiCl_3$ becomes significant above 1800K.

Figs. IV-7-9 show the calculated CVD phase diagrams for the system when H_2 is included as a carrier gas. In these diagrams, phase fields of C(s); β-SiC; β-SiC+C(s); Si(s)+β-SiC; Si(ℓ) +β-SiC; Si(s); and Si(ℓ) are observed. Under certain conditions, especially low temperatures, no condensed phases are deposited. Referring to the conditions for the deposition of single phase β-SiC in this system, there are several implications for CVD processors. If one desired to work at low system pressures (LPCVD) to minimize contamination, one should avoid high H_2 carrier gas concentrations, where the conditions for single phase β-SiC deposition are limited (compare Figs. IV-7(d) and IV-9(d)). Rather, one should work at lower carrier gas concentrations, and at Si/Si+C $\gtrsim$ 0.6 in the input gas. At system pressures around 1 atm, conditions are less limited, with high H_2 carrier gas concentrations allowing a wide choice of temperatures and Si/Si+C parameters (Fig. IV-9).

Table IV-III. $SiCl_4/CCl_4$ System: Equilibrium Gas Phase Composition at 1 atm pressure* (Si/Si+C = 0.5)

Species	Species Partial Pressure (atm)	
	AT 1000K	AT 2000K
Si	$< 10^{-20}$	0.71×10^{-14}
$SiCl_4$	0.33	0.25
$SiCl_3$	0.22×10^{-8}	0.82×10^{-2}
$SiCl_2$	0.67×10^{-17}	0.41×10^{-4}
SiCl	$< 10^{-20}$	0.12×10^{-9}
Cl	0.33×10^{-3}	0.42
Cl_2	0.66	0.32
CCl_4	0.30×10^{-2}	0.38×10^{-5}
CCl	$<10^{-20}$	0.19×10^{-7}

*Total system pressure

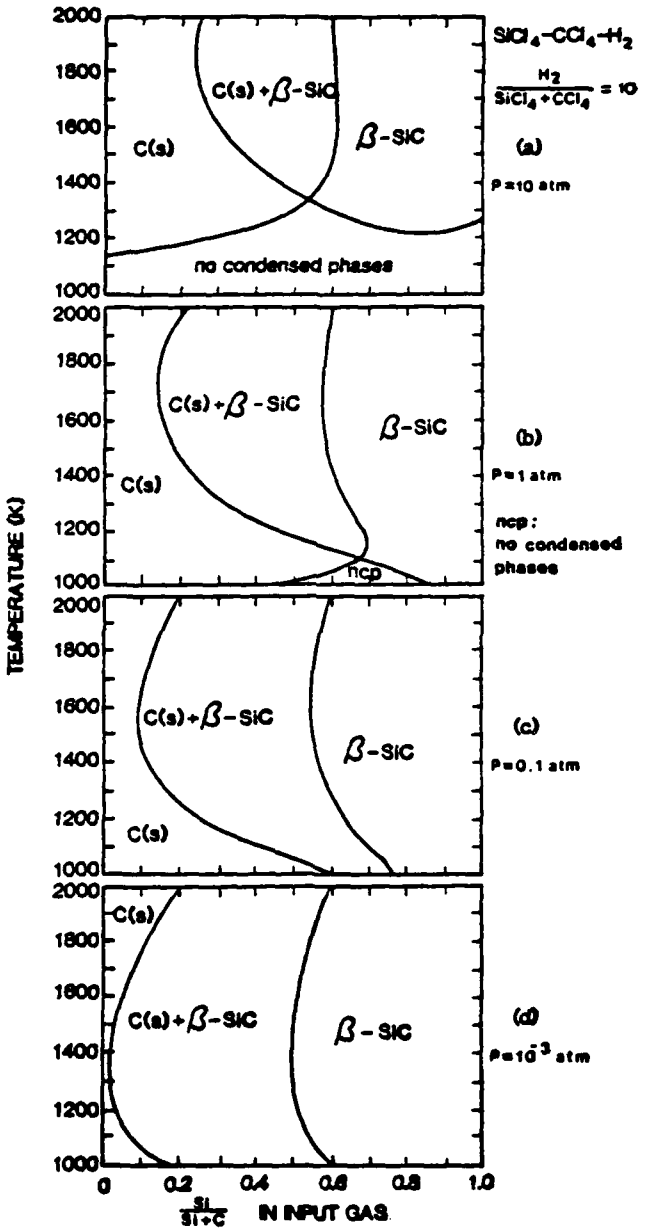

Figure IV-7. The $SiCl_4/CCl_4/H_2$ system at various total pressures, with $H_2/(SiCl_4 + CCl_4) = 10$.

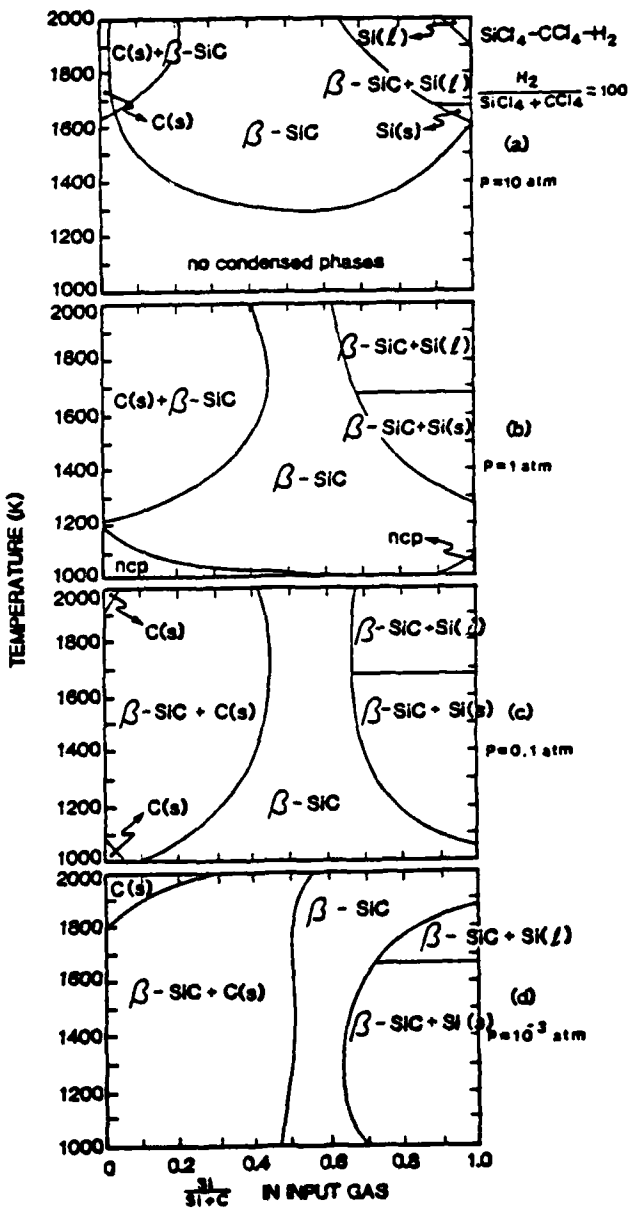

Figure IV-8. The $SiCl_4/CCl_4/H_2$ system at various total pressures, with $H_2/(SiCl_4 + CCl_4) = 100$.

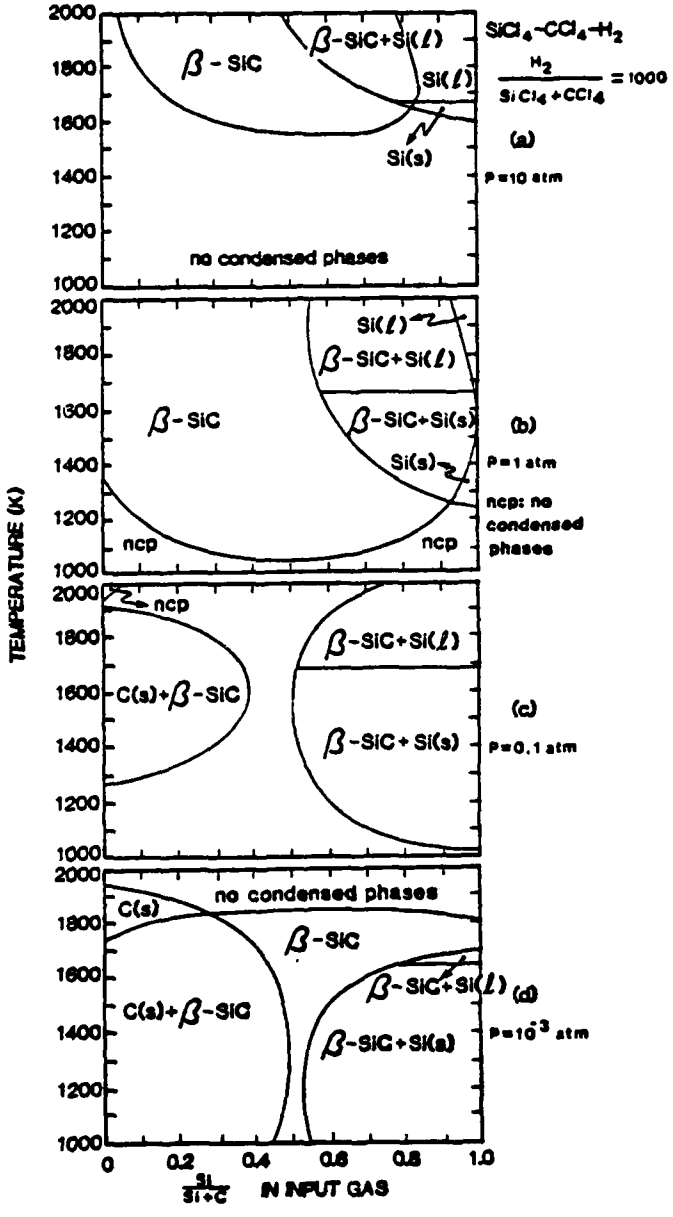

Figure IV-9. The $SiCl_4/CCl_4/H_2$ system at various total pressures, with $H_2/(SiCl_4 + CCl_4) = 1000$.

In terms of competing equilibria, the following are valid at the lower temperatures:

$$SiCl_4 + CCl_4 + 4H_2 \rightleftarrows \beta\text{-}SiC + 8HCl \qquad \text{equ. (7)}$$

$$CCl_4 + 2\,H_2 \rightleftarrows C(s) + 4HCl \qquad \text{equ. (8)}$$

$$SiCl_4 + 2H_2 \rightleftarrows Si(s) + 4HCl \qquad \text{equ. (9)}$$

In the $SiCl_4/CCl_4/CCl_4/H_2$ system, the CVD phase diagrams show that it is possible to establish conditions such that any one of the equilibria is predominantly to the right, while the remaining two are completely to the left. At low H_2 gas concentrations, competition for the reactant gases is primarily between equilibria 7 and 8 (Fig. 7), while at higher H_2 concentrations it is also necessary to consider equilibrium (9) (see Fig. IV-8 and IV-9), as condensed Si phases also occur.

Typical species present in the gas phase at low and high temperatures are given in Table IV-IV. At the higher temperatures, equ. (7)-(9) again do not completely describe all the species present in the gas phase. As noted previously, this does not affect the logic of the above discussion.

(5) The $SiCl_4/CH_4/H_2$ System

At high H_2 carrier gas concentrations this system is similar to that of $SiCl_4/CCl_4/H_2$ discussed above. The $SiCl_4/CH_4$ system without H_2 carrier gas is shown in Fig. IV-10. Although β-SiC is deposited, there are no β-SiC single phase fields. The system shows only a small pressure effect (Fig. IV-10).

(6) The $CH_3SiCl_3H_2$ System

The CVD phase diagrams for the methyltrichlorsilane/hydrogen system are shown in Figs. IV-11(a)-11(c). Note that for this system the Si/Si+C ratio is fixed (0.5), and the diagrams are presented with $H_2/(CH_3SiCl_3)$ mole ratio as the abscissa. The results show that the system is not very pressure dependent, and that a quantity of H_2 carrier gas is required in order to deposit β-SiC alone - up to 100 moles H_2 per mole CH_3SiCl_3 (Fig. IV-11(c)). At lower H_2 carrier gas concentrations, C(s) is codeposited.

Table IV-IV. $SiCl_4/CCl_4/H_2$ System: Equilibrium Gas Phase Composition at 1 atm pressure* (Si/Si+C = 0.5, $H_2/(SiCl_4 + CCl_4)$ = 10)

Species	Species Partial Pressure (atm)	
	At 1000K	At 2000K
H	0.19×10^{-8}	0.13×10^{-2}
H_2	0.73	0.68
SiH_4	0.29×10^{-11}	0.30×10^{-7}
CH_4	0.45×10^{-1}	0.18×10^{-3}
C_2H_4	0.25×10^{-6}	0.25×10^{-5}
CH_3	0.25×10^{-8}	0.88×10^{-5}
C_2H	0.54×10^{-18}	0.14×10^{-5}
C_2H_2	0.79×10^{-9}	0.60×10^{-3}
SiH	0.94×10^{-19}	0.13×10^{-5}
Si	$< 10^{-20}$	0.23×10^{-5}
$SiCl_4$	0.45×10^{-1}	0.94×10^{-4}
$SiCl_3$	0.21×10^{-3}	0.29×10^{-2}
$SiHCl_3$	0.86×10^{-4}	0.22×10^{-4}
$SiCl_2$	0.45×10^{-6}	0.14×10^{-1}
SiH_2Cl_2	0.33×10^{-5}	0.14×10^{-4}
SiH_3Cl_3	0.69×10^{-5}	0.39×10^{-4}
SiCl	0.34×10^{-15}	0.38×10^{-4}
Cl	0.46×10^{-9}	0.44×10^{-3}
Cl_2	0.13×10^{-11}	0.34×10^{-6}
HCl	0.18	0.30
CH_3Cl	0.41×10^{-6}	0.55×10^{-6}
CCl_4	$< 10^{-20}$	0.44×10^{-17}
CCl	$< 10^{-20}$	0.19×10^{-10}

*Total system pressure

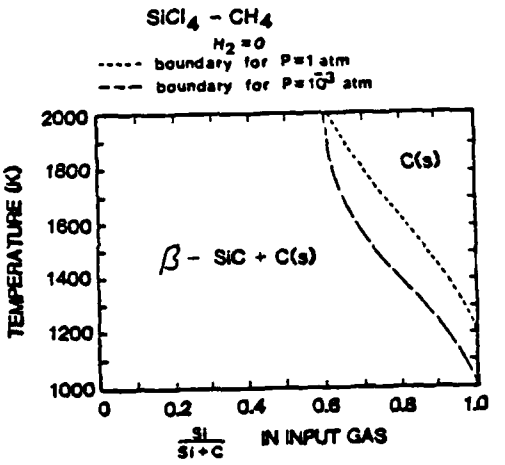

Figure IV-10. The $SiCl_4/CH_4$ system with no carrier gas.

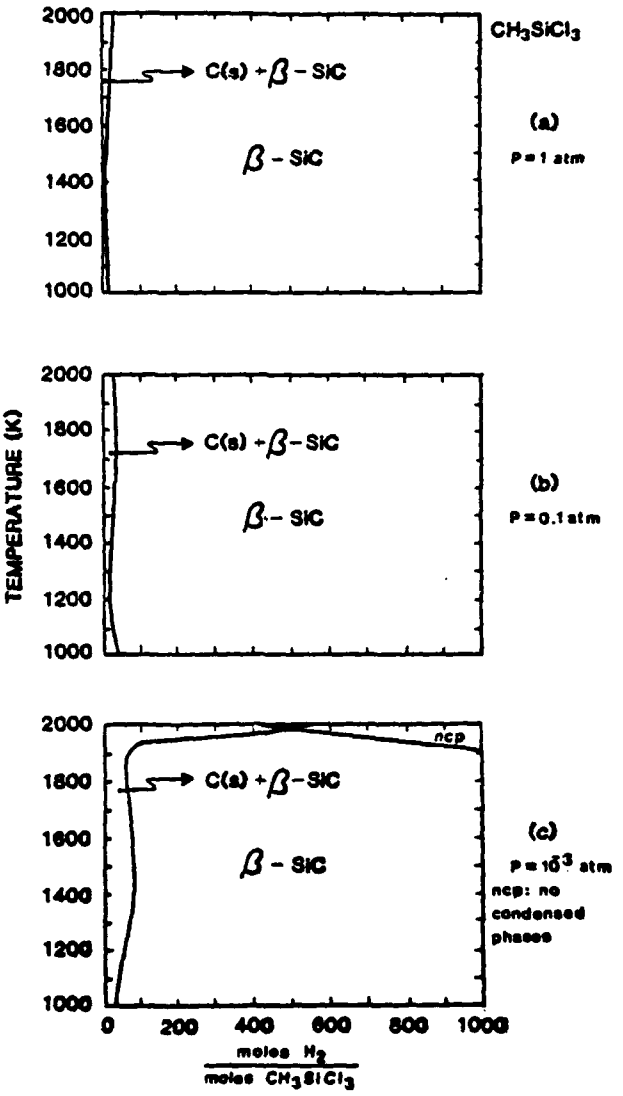

Figure IV-11. The CH_3SiCl_3/H_2 system at various total pressures.

Additional calculations also show that in the CH_3SiCl_3/Ar system, C(s) codeposited with β-SiC under all conditions. This is consistent with the role of Ar discussed earlier.

(7) The $(CH_3)_2SiCl_2/H_2$ System

In the case of the dimethyldichlorosilane/hydrogen system (Figs. IV-12(a)-(c)) the conditions for single phase β-SiC deposition are substantially more limited due to the lower Si/Si+C ratio of 0.33. It is necessary to operate at system pressures around 1 atm. Even then, it is also necessary to operate at high H_2 carrier gas concentrations and moderate temperatures as shown in Fig. IV-12(a).

DISCUSSION

(1) Comparison with Previous Calculations

Some calculated results have appeared in the literature which are relevant to the CVD of silicon carbide. In general, however, these have not been presented as CVD phase diagrams.

Minagawa and Gatos (60) have performed some calculations for the $SiH_4/C_3H_8/H_2$ system. The thermodynamic conditions employed by these authors were much more limited but within the values used in the present research. In the area of overlap the results appear to be in agreement. However, at one set of conditions these authors have shown three condensed phases in equilibrium. This is not possible according to the phase rule. The authors have assumed that α is not predominant SiC phase if α-SiC substrates are used. β-SiC was not considered.

Lever, (62) considering the gas phase only, has calculated equilibrium compositions in the Si-H-Cl system. With one exception, there is agreement with the values of the species concentrations calculated in the present work where the Si/Si+C ratios are approximately one. However, he has omitted the species $SiCl_3$, which the present work shows is significant.

Turpin and Robert (63) have performed some calculations for the $CH_3SiCl_3/CH_4?H_2$ system. Their predications for the phases which would

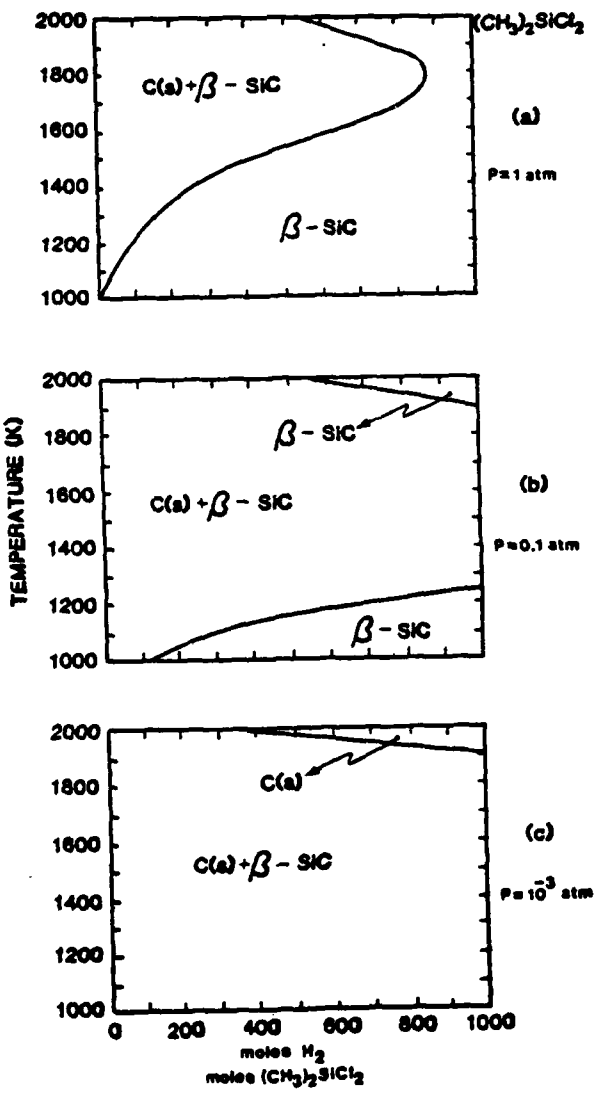

Figure IV-12. The $(CH_3)_2SiCl_2/H_2$ system at various total pressures.

deposit appear to be in agreement with the present work for the case where there is no methane in the input gas. The results of Christin et al., (64) are in close agreement with those of the present work for the CH_3SiCl_3/H_2 system.

Pampuch and Stobierski (65) have quoted the calculated work of Kuznetsov et al., giving values of Si/Si+C for which single phase SiC can be found in the temperature range 1773-2073K. The Cl/H ratio is given as approximately 0.1, but no pressure is quoted. A system pressure of 1 atm. is therefore assumed. The results are comparable with Fig. IV-8(b). However, the latter diagram has been calculated using a smaller Cl/H ratio, and, it should be remembered that the system is very dependent on H_2 content and pressure. Pampuch and Stobierski (65) have also compared these results with the empirically determined silicon carbide single phase regions reported by Wessels, Gatos and Witt (66). This comparison is not valid, as the latter refers to the $SiH_4/C_3H_8/H_2$ system. The present results have shown this system to be substantially different from those which contain chlorine.

(2) Comparison with Experimental Literature

The original intention of the authors was to make a detailed comparison of the present calculated CVD phase diagrams with experimental data reported in the literature in order to determine the usefulness of the thermodynamic equilibrium method for CVD processing. However, the following problems were encountered:

(i) The range of conditions covered for a particular experimental system has generally been small.

(ii) In very few cases have all the necessary experimental conditions been published. Typically the carrier gas concentrations and/or flow rates have been omitted. The present results have demonstrated the dependence on all the parameters; pressure, temperature, Si/Si+C ratio, and carrier gas concentration.

(iii) Experimentally, it is difficult to observe small quantities of second phase material codeposited with the silicon carbide. This has been emphasized by Popper (67). Avigal et al. (68) have reported that frequently free C is deposited which cannot be observed by powder XRD, but which can be observed by microchemical analysis. Thus, experimental reports of the extent of the single phase or the 2-phase regions may be in error, depending upon the analytical technique used.

The work of Harris et al.(69) is most easily compared with the present results. These workers calculated and determined experimentally CVD phase diagrams for the SiH_4/C_3H_8 system for a limited range of conditions. Agreement between experimental and calculated results, and also with the present data, is very good. It is interesting to note that these authors report a change in the SiC from single crystallinity to polycrystallinity at the outset of the deposition of small quantities of a second phase.

For the reasons given above, comparison with other results reported in the literature must necessarily be more qualitative. The observation that at high H_2 mole ratios the control of the silane/hydrocarbon ratio in the input gas is less critical, has been reported in the lieterature (70). The codeposition of C with SiC at low Si/Si+C ratios in the Si-C-H system, as reported in this work, is consistent with results which have appeared in the literature (69, 70). However, there are reports of the extension of the β-SiC single phase field to higher Si/Si+C ratios than calculated in the present work prior to the codeposition of Si (69, 70).

In the important CH_3SiCl_3/H_2 system, there are some conflicting literature reports of the phases codeposited with β-SiC. The results of Popper and Riley (67), Koboyashi et al. (71), and Gulden (72), appear to be in agreement with the present work, as C is reported to codeposit with SiC under the conditions specified. In contrast, von Muench and Pettenpaul (73), and Turpin and Robert (63) have reported that Si can be codeposited with SiC under certain conditions, which is not in

agreement with the results of the above workers, or with the present thermodynamic calculations for the CH_3SiCl_3/H_2 system. Chin et al. (74) have published an experimental CVD phase diagram for the CH_3SiCl_3/H_2 system. The reported conditions whereby β-SiC and C(s) are codeposited appear to be in fair agreement with the present work. However, they also report the presence of free Si at high H_2 carrier gas concentrations, but it should be noted that free C is also present, indicating non-equilibrium conditions. Weiss and Diefendorf (75) have reported the codeposition of SiC and C at high temperatures (~1900K), and the codeposition of SiC and Si at lower temperatures around 1500K, both regions being observed at fairly low H_2/CH_3SiCl_3 ratios (between 4 and 1). Their high temperature result is in agreement with the present work, but the low temperature is not (see Fig. IV-11(a)).

In the dichlorodimethylsilane system, Ivanova et al. (76) have reported the codeposition of SiC and C over a wide range of conditions. This is in agreement with the present calculations, but conflicts with reports by Rai-Choudhury and Formingoni (77) that SiC and Si can be codeposited.

(3) Additional Remarks

The work described above has assumed that equilibrium conditions exist within the vessel. This is necessarily an approximation in an open system with a finite flow of reactant gases in, and product gases out. However, the kinetics of the decomposition reactions, and the diffusion of species on the substrate to form the condensed phases, is normally so fast, that the system can be controlled by the equilibria described above. Under these conditions, the thermodynamic equilibrium calculations provide an extremely useful description of the composition of the phases condensing on the heated substrate, and of the composition of the gas phase in the boundary layer adjacent to the substrate. Good agreement between calculation and experiment has also been reported by Wan and Spear (68) in the compex Nb-Ge-H-Cl system. In some systems under particular experimental conditions, poor agreement between experimental results and thermodynamic equilibrium calculations suggests that kinetic factors can be controlling the deposition process (78, 79).

Factors such as the relative decomposition rates of the gaseous precursors, and the relative "sticking coefficients" of the gaseous species to the heated substrate become important.

Bernard (78) has recently reviewed the application of thermodynamics to CVD and modelling methods which include a consideration of kinetic effects. He pointed out that a thermodynamics analysis must be completed before kinetic effects are considered, and that "a thermodynamic analysis must be part of a study of every chemical or physical step involved in CVD "

Inclusion of kinetic effects in the calculations described above are outside the scope of the present work - the systems are too complex with too many gaseous species and condensed phases. Instead, the author believes that the CVD phase diagrams presented above are of fundamental importance for showing the range of conditions generally available to processors of SiC by CVD.

The concentrations of the condensed phases allow one to calculate "the theoretical deposition efficiency" of a given condensed phase under the conditions considered. This term has been defined as the number of moles of a condensed phase which would deposit under thermodynamic equilibrium conditions divided by the maximum number of moles of the same phase which could be formed by the input gas if there were no thermodynamic or kinetic limitations (80). Analysis of the present data shows the following:

(i) The deposition efficiency of β-SiC with the β-SiC single phase fields is generally high, typically > 0.90. For example, in the CH_3SiCl_3/H_2 system, the theoretical SiC deposition efficiency between 1400K and 2000K varies from 0.98 at low H_2 carrier gas concentrations to 0.94 at high H_2 concentrations. Only at temperatures below 1300K does the deposition efficiency fall, reaching 0.73 at 1100K, and 0.5 at 1000K (1 atm system pressure).

(ii) Deposition efficiency does fall as one approaches the conditions under which no condensed phases are formed. Deposition efficiency is therefore > 0.95 in the $SiH_4/CH_4/H_2$ system wherever single phase β-SiC is formed, the only exception being the conditions

shown in Fig. IV-4(d), where the efficiency falls as one approaches the region of no condensed phases, i.e., it is 0.73 at 1800K. In the $SiCl_4/CCl_4/H_2$ system, the regions of no condensed phases are much more extensive, and the deposition efficiency in adjacent β-SiC single fields is lowered accordingly. This is particularly marked under the conditions shown in Figs. IV-8(a) and IV-9(b), i.e. high pressure and high H_2 carrier gas concentration.

(iii) The β-SiC deposition efficiency within two-phase fields varies from 0 to 1.

It should be noted that only the most stable condensed phases have been considered in the present work. At low temperatures in particular, amorphous and other metastable condensed phases may be formed. The substrate type also has an effect, the use of α-SiC substrates promoting the growth of α-SiC films at high temperature (70).

SUMMARY

CVD phase diagrams have been calculated for the preparation of SiC from commonly used gaseous precursors. The results show that single phase β-SiC deposition is strongly influenced by operating conditions for both the Si-C-H and Si-C-H-Cl systems. Optimum conditions for single phase deposition have been discussed.

Comparisons of the present calculated results with literature data is difficult, primarily due to limited and contradictory experimental data. The present calculated CVD phase diagrams therefore show general agreement with some authors, but disagreement with others. Examples of disagreement are with regard to the extent of the β-SiC single phase field in the SiH_4/hydrocarbon/H_2 systems at high SiH_4 concentration in the input gas, and the possibility of Si codeposition with β-SiC in the $(CH_3)_2SiCl_2/H_2$ and CH_3SiCl_3/H_2 systems.

The transition from equilibrium- to kinetically-controlled CVD processes have been discussed briefly. This work emphasized the fundamental importance of the thermodynamic equilibrium description of the SiC CVD system in providing an understanding of the system and as an approach to setting up the CVD process.

B. CVD Thin Films of Beta Silicon Carbide

The epitaxial growth of β-SiC on Si substrates has been achieved. Although several approaches were attempted, a two-step process involving the chemical conversion of the heated Si surface to β-SiC using flowing C_2H_4 in H_2 followed by the CVD of β-SiC using SiH_4 and C_2H_4 in H_2 was the most successful. Reproducible results can be obtained by the two-step growth process. However, it was very difficult to grow reproducible films of β-SiC using only the latter one-step CVD process.

1. Material Defects and their Characterization and Cause

Figure IV-13 reveals defects on the grown surface of the single crystal β-SiC films. Triangular pyramids are observed on all epitaxial films with (111) orientation, while rectangular hillocks are revealed on all epitaxial films with (100) orientation. The shape of the defects is believed to be determined by the symmetry of the substrate surface. Moreover, crack lines are also observed but only in the epitaxial β-SiC films deposited on the Si(111) substrates, as shown in Fig. IV-13(a).

There is also a significant difference between the surface morphologies of the epitaxial films and the polycrystalline films of β-SiC. The top surface of the epitaxial β-SiC films is very smooth although this characteristic does have a slight dependence on the degree of off-axis orientation of the Si substrate. The top surface of a polycrystalline β-SiC film is very rough with a granular appearance. However, the bottom surface of this β-SiC film at the Si/SiC interface is much more smooth because it is against the mirror-like surface of the Si substrate.

In some cases, part of the Si substrate edge extended beyond the β-SiC film whenever the former material was fractured to produce samples for scanning electron microscopy. Figure IV-14(a) and (b) are SEM micrographs showing both the β-SiC grown film and the Si substrate top surfaces for two different orientations. It is interesting to note that triangular pits were found on the Si(111) substrate top surface, while rectangular pits were observed on the Si(100) substrate top surface. The orientation and shape of the pits correlate well to those

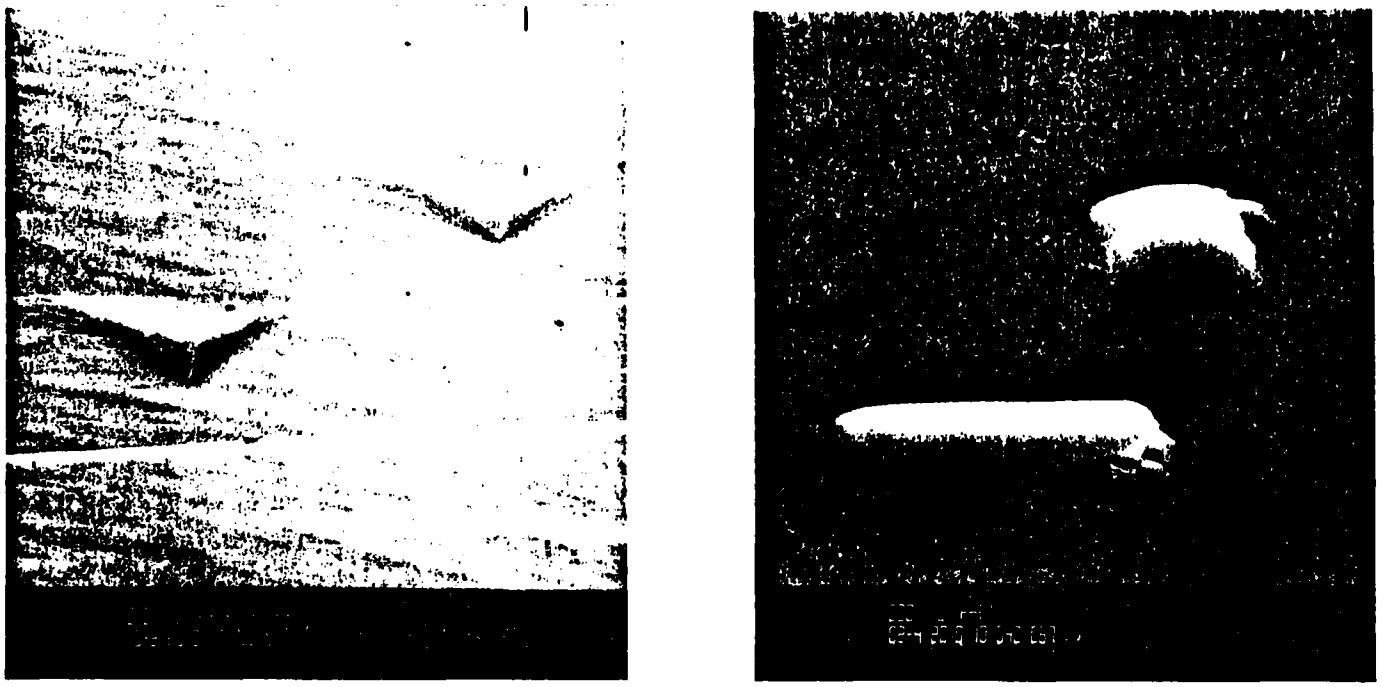

(a) (b)

Figure IV-13. SEM micrographs showing defects on the top surface of the β-SiC epitaxial films grown on (a) the Si(111) and (b) the Si(100) substrates.

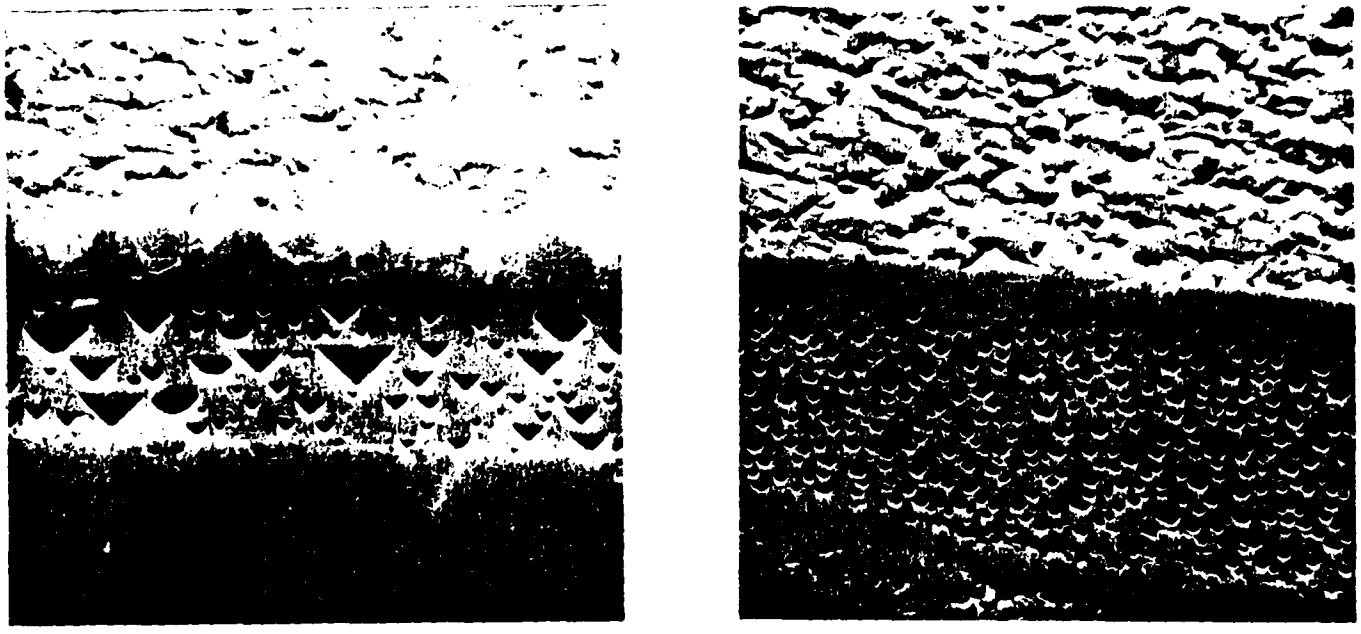

(a) β-SiC / Si(111)

(b) β-SiC / Si(100)

Figure IV-14. SEM micrographs showing the β-SiC grown film surface (top portion of the photographs) and the Si substrate upper surface and the fractured side surfaces (bottom portion of the photographs). (4000x)

of the crystallites observed on the corresponding β-Sic film surface.

The pits observed on the Si substrate top surface after the β-SiC deposition were not caused by the HCl gas phase etching because no HCl pre-etch was employed prior to the epitaxial growth when the chemical conversion step was employed. The pitted Si surface may be caused by the thermal etching of this surface at high temperature and/or by the chemical conversion of Si at the initial stage of the two-step growth process. In order to further examine this mechanism, several (111) and (100) wafers were heated to 1330°C under atmospheric pressure within a flow of H_2 and held at that high temperature for 10 min. then cooled to room temperature in the reactor chamber. No such pits were found on any of the Si surfaces. This eliminated the possibility that the pits resulted from the evaporation of Si atoms at high temperature.

Another experiment was carried out by using only the chemical conversion technique. Silicon substrates with (111) and (100) orientations were heated from room temperature to 1330°C for 3 min. under a 1 sccm flow of C_2H_4 and 3000 sccm flow of H_2 at a total pressure of 760 Torr. The SEM micrographs presented in Fig. IV-15 show that the Si substrates were covered by a very thin layer of deposit. The characteristic voids also revealed in the micrographs are on the Si surface and therefore underneath the chemically converted layer. The triangular shaped voids seen in Fig. IV-15(a) occurred when Si(111) was used as the substrate. The voids were also different in size. In certain places, two voids touched and tended to grow larger by merging together. Figure IV-15(b) shows that rectangular shaped voids of different sizes occurred when Si(100) was used as the substrate. The density of these characteristic voids was considerably less on the Si(100) substrate than on the Si(111) substrate. It is believed that the formation of these voids is related to the growth mechanism involved in the chemical conversion of the Si substrate. It apparently suggested that the Si atoms from the substrate diffuse out through the converted layers to react with the C atoms at the outermost surface (i.e., the growth surface) and, therefore, leave behind a void in the Si substrate at the β-SiC/Si interface.

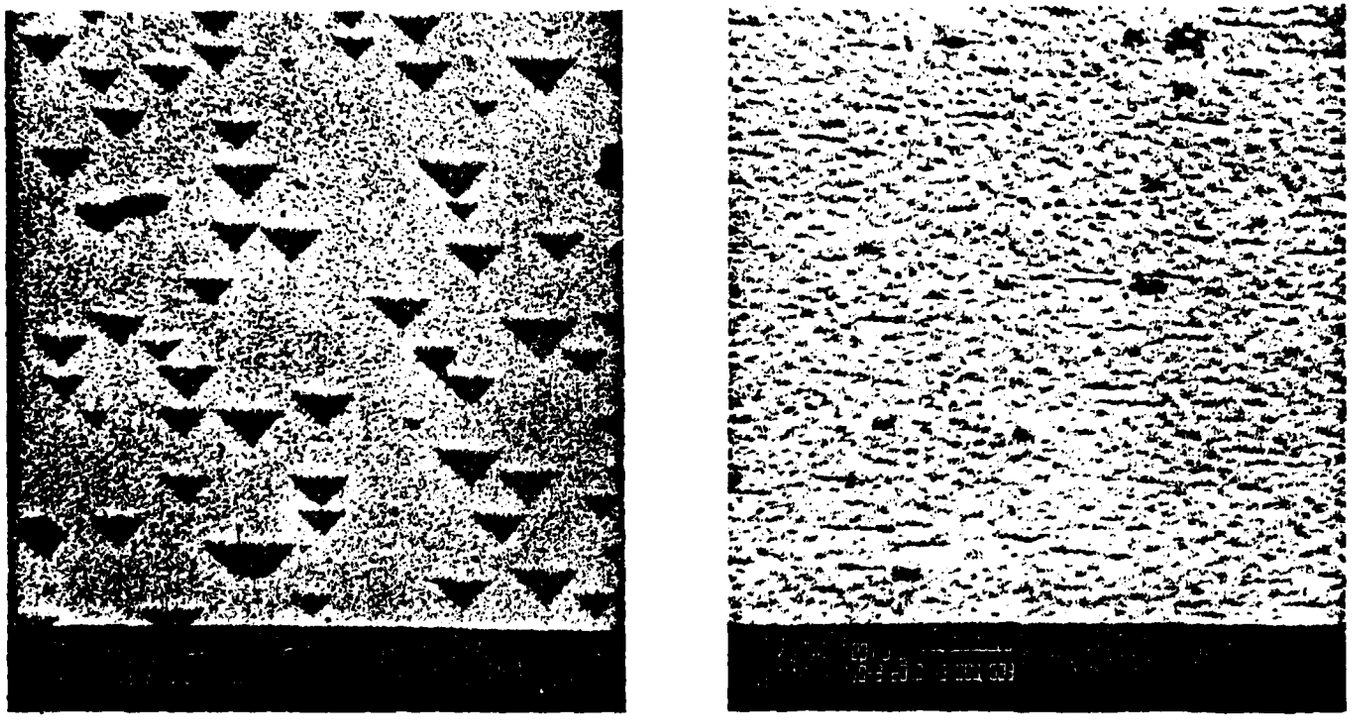

(a) Si(111)

(b) Si(100)

Figure IV-15. SEM micrographs of the chemically converted Si surface after a 3 min chemical conversion conducted from room temperature to 1330°C with C_2H_4=1 sccm and H_2=3000 sccm and a total pressure of 760 Torr.

2. X-ray and Electron Diffraction

Figure IV-16 shows the x-ray diffraction spectrum of an epitaxial β-SiC film grown on a Si(111) substrate. In this 2θ scan from 20° to 80° using a Cu target, there appear to be more peaks than one should expect from just Si and β-SiC. The β-SiC(111), the β-SiC(222) as well as the Si(111) peaks resulting from the $Cu_{K\alpha}$ and $Cu_{K\beta}$ radiations are easy to identify. By scanning the pure Si(111) substrate along, all of the extra peaks can thus be identified and result from other characteristic radiations, e.g., those of Fe, Cr and W. These elements are the contaminants of the Cu target in the x-ray tube. Table IV-5 summarizes the 2θ values for each possible diffraction. Thus, all the peaks can now be indexed as shown in Fig. IV-16. It is interesting to note that a double reflection of the Si(222) peak from the $Cu_{K\alpha_1}$ and $Cu_{K\alpha_2}$ occurs in this case; as a rule, this phenomenon is normally absent. Furthermore, the β-SiC(222) peaks from the $Ci_{K\alpha_1}$ and $Cu_{K\alpha_2}$ can be easily resolved in the spectrum. An enlarged diffraction spectrum of the β-SiC(222) peaks is presented in Fig. IV-17. The presence of this dual β-SiC(222) peak is also an indication of the excellent quality of the single crystallinity of the grown β-SiC film.

Figure IV-18 shows a 2θ scan from 44° to 62° for an epitaxial β-SiC film grown on a Si(111) substrate. In this 2θ range, the (222) peaks resulting from both the β-SiC film and the Si substrate are included if the sample is tilted 35° on the Schulz goniometer so that the (220) is the diffracting plane. Rotating the sample one turn about the AA' axis (see Fig. III-4), one can detect three peaks of β-SiC(220) reflections which are separated 120° from each other. This indicates the normal 3-fold symmetry of the (220) about the <111>. One may conclude from this study that the crystal structure of the grown β-SiC(111) film is indeed single crystal in nature.

As for the β-SiC film grown on the Si(100) substrate, Fig. IV-19 shows the Si(400) and β-SiC(200) peaks resulting from the $Cu_{K\alpha}$ and the and the $Cu_{K\beta}$ radiations and the β-SiC(200) peaks from the $Fe_{K\alpha}$ and the $Fe_{K\beta}$ radiations. Figure IV-20 is the 2θ scan from 45° to 62° for an

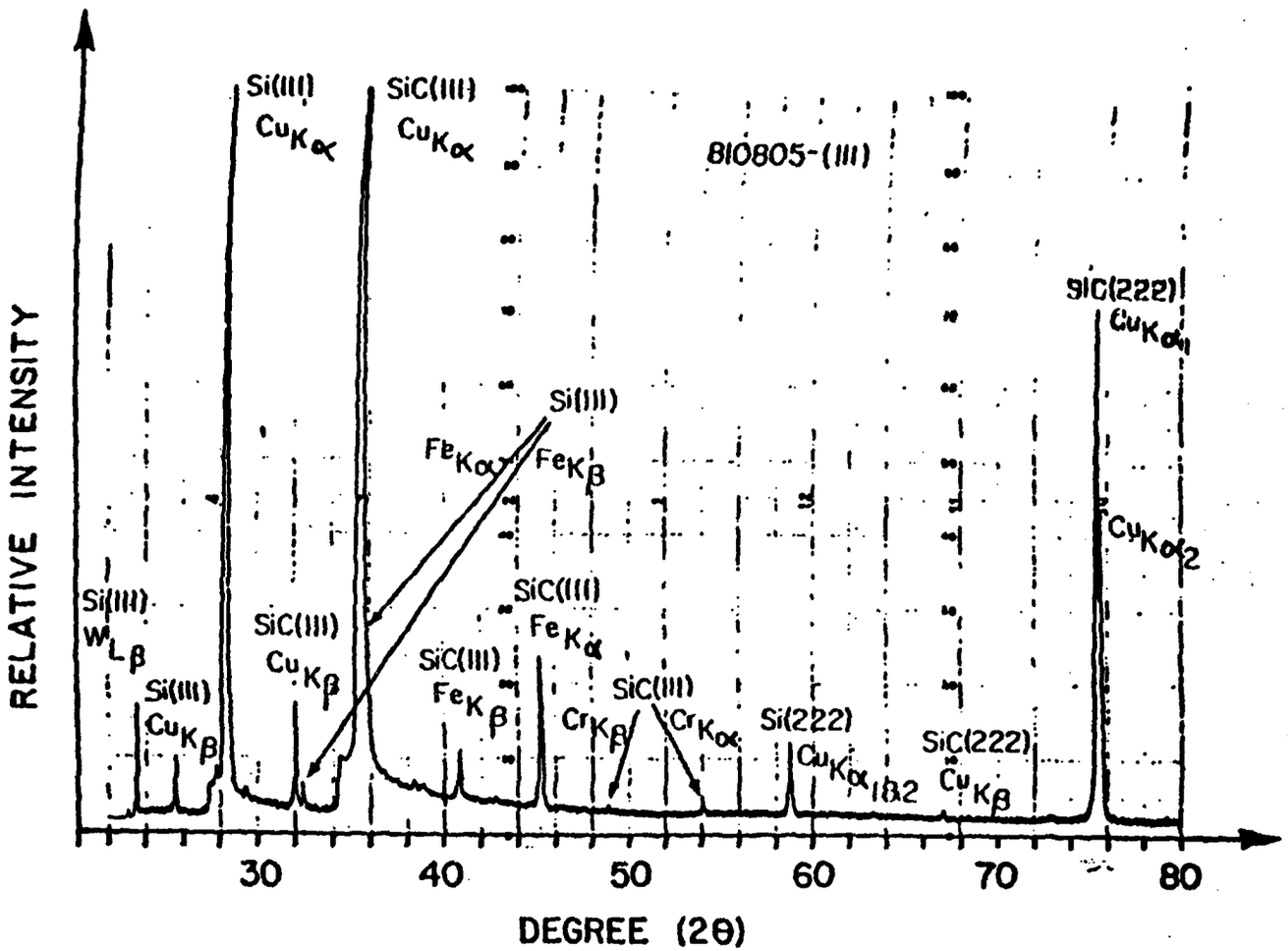

Figure IV-16. X-ray diffraction spectrum showing the epitaxial growth of a 3μ thick β-SiC film on a Si(111) substrate. A substantial number of peaks representing only a few particular planes of Si and SiC have resulted because of the several impurity elements (Fe, Cr and W) in the target in the x-ray tube.

Table IV-5. Two-theta values for each possible diffraction which could occur from certain refraction planes as a result of characteristic radiation from impurity elements in the Cu target in the x-ray tube.

Radiations		2θ (degree)				
	Wavelength λ (Å)	Si(111)	β-SiC(111)	Si(400)	β-SiC(200)	β-SiC(222)
$Cu_{K\alpha}$	1.5418	28.44	35.77	69.23	41.62	
$Cu_{K\beta}$	1.3922	25.63	32.20	61.72	37.42	
$Fe_{K\alpha}$	1.93728	35.96	45.40	91.09	53.02	
$Fe_{K\beta}$	1.75653	32.51	40.96	80.66	47.75	
$W_{L\alpha_1}$	1.47635	27.21	34.21	65.91	39.77	
$W_{L\alpha_2}$	1.28176	23.60	29.59	56.36	34.36	
$Cr_{K\alpha}$	2.2909	42.80	54.30	115.15	63.72	
$Cr_{K\beta}$	2.0848	38.80	49.08	100.38	57.42	
$Cu_{K\alpha_1}$	1.5405			69.17		75.37
$Cu_{K\alpha_2}$	1.5443			69.36		75.59

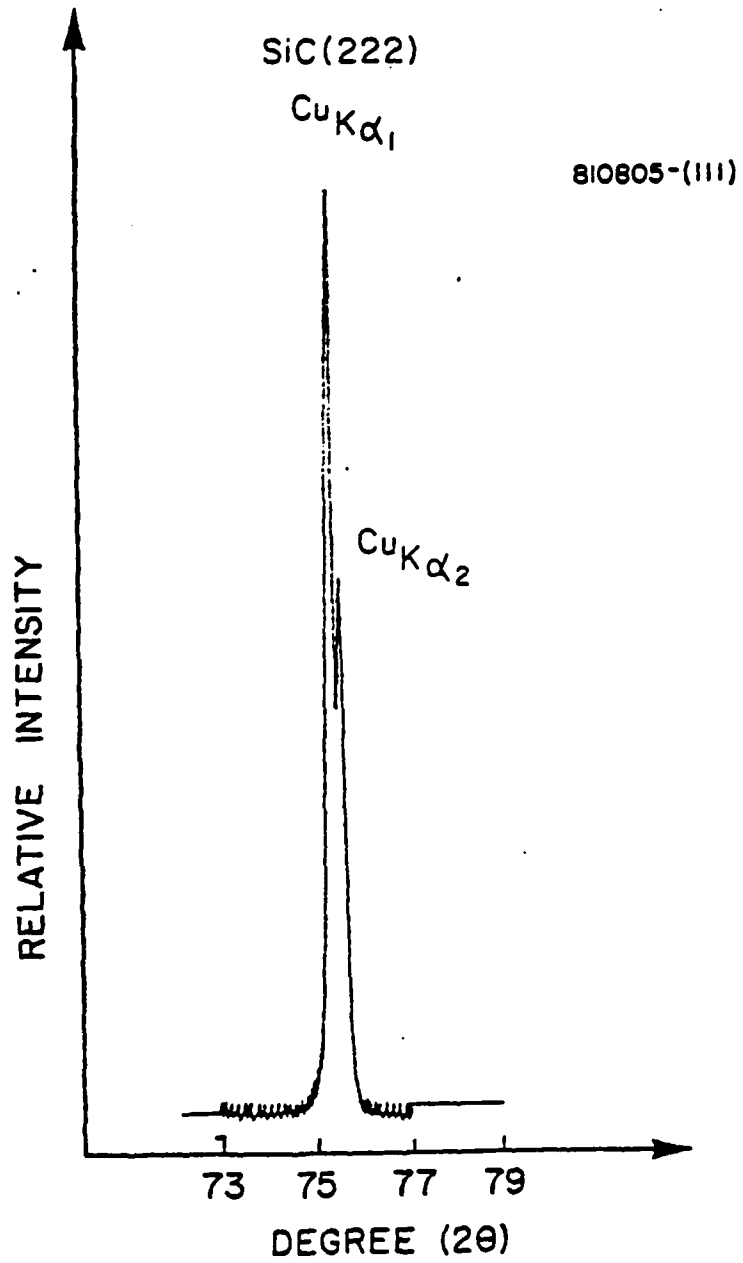

Figure IV-17. X-ray diffraction spectrum of β-SiC(222) showing the dual-peak resulting from the K_{α_1} and K_{α_2} radiations of the Cu target in the x-ray tube.

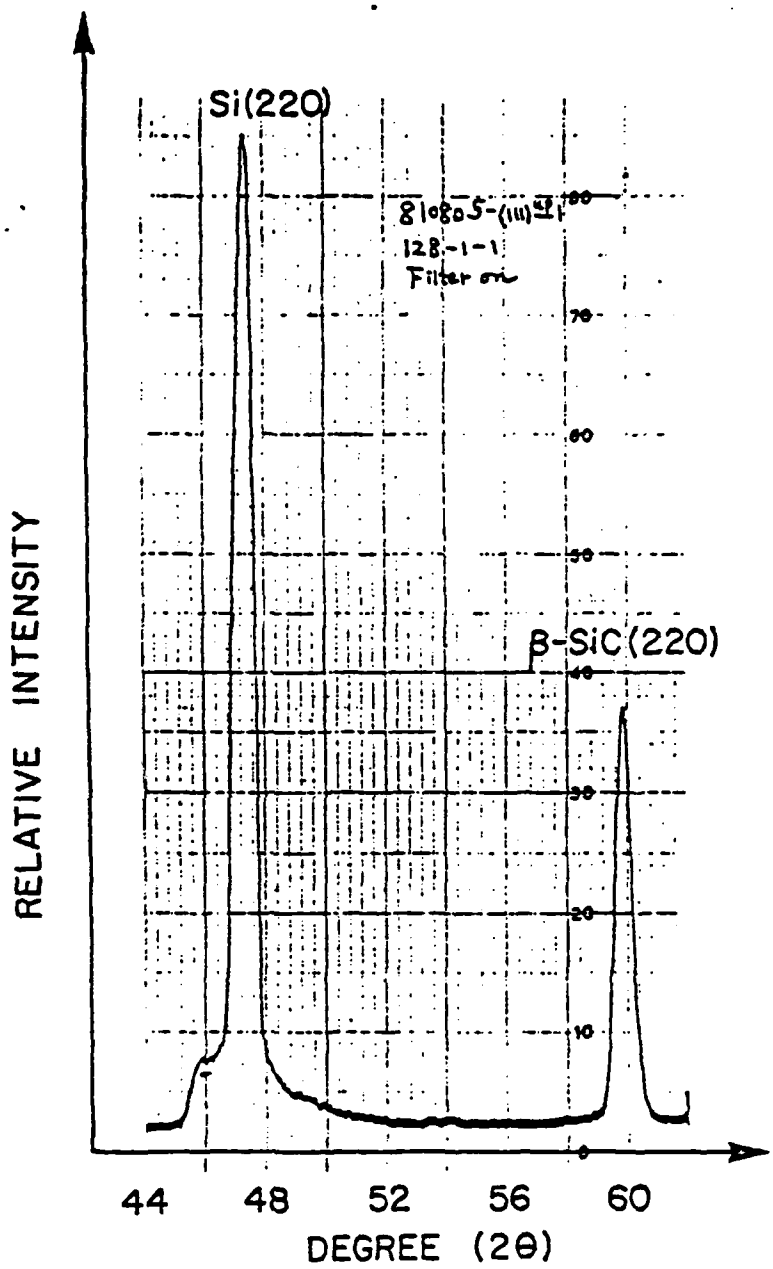

Figure IV-18. The x-ray diffraction spectrum of an epitaxial β-SiC thin film grown on the Si(111) substrate. This sample was first tilted 35° on the Schultz goniometer and then scanned from 44° -62°.

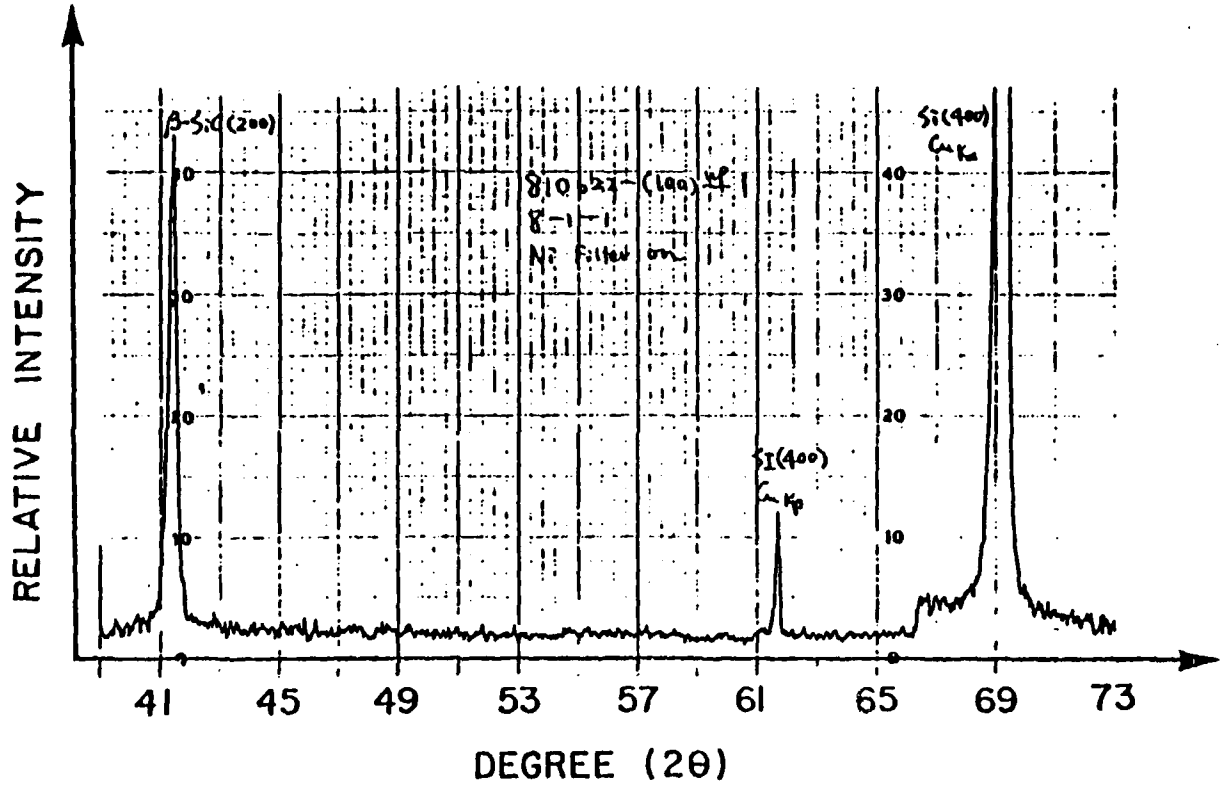

Figure IV-19. X-ray diffraction spectrum which indicates the existence of the epitaxial growth of a β-SiC film on a Si(100) substrate.

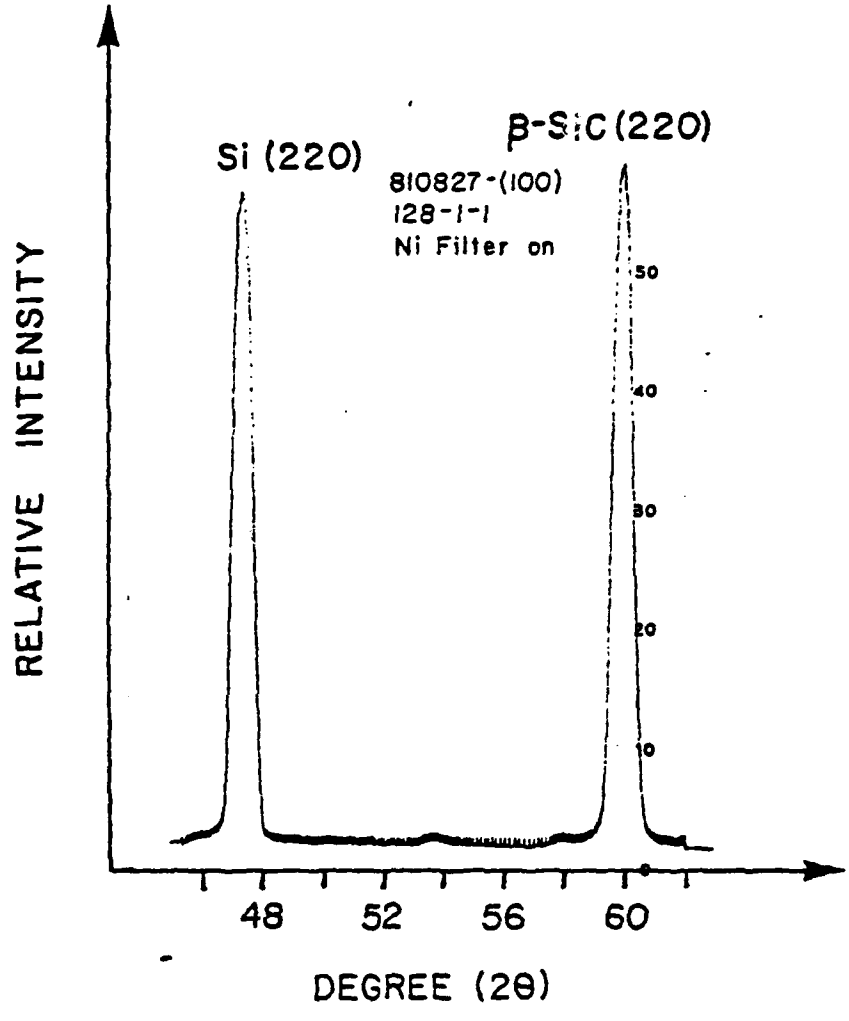

Figure IV-20. The x-ray diffraction spectrum of an epitaxial β-SiC thin film grown on a Si(100) substrate. This sample was first tilted 45° on the Schultz goniometer and then scanned from 45° -62°.

epitaxial β-SiC film grown on a Si(100) substrate. As in the example noted above, the (220) again becomes the principal diffracting plane when the sample is tilted 45° about BB' axis (see Fig. III-4). However with the Si(100) substrate orientation, the β-SiC(220) peaks are monitored at a 90° separation because of the 4-fold symmetry of (220) about <100>. The presence of this symmetry as revealed by the diffraction pattern allows one to conclude that the crystal structure of the grown β-SiC(100) film is also a single crystal.

Figure IV-21 shows samples used in the x-ray transmission Laue research. The center area of the Si substrate was etched away selectively by a mixture of HF and HNO_3. The epitaxial β-SiC films were transparent with a light yellowish color which is typical of high purity crystals and films of this material.

The transmission Laue pattern (TLP) for an epitaxial β-SiC film grown on a Si(111) substrate is shown in Fig. IV-22(a). It is obvious that the Laue spots for the β-SiC(111) film have a 3-fold symmetry. Because of the difficulty in clearly printing the whole pattern, the same TLP containing the additional but weaker spots plotted from the x-ray negative is shown in Fig. IV-22(b). The results of the indexing procedure were also verified by using a Leonhardt chart and a standard (111) sterographic projection for an FCC structure. Most of the Laue spots could be routinely indexed; however, 12 spots contained in three groups of four spots each and very close to the three (111) spots were more difficult to identify. Further investigation showed that these satellite-like spots were on three zone axes and on two rings which corresponded to the β-SiC(111) reflections from the K_α and K_β characteristic radiations of the Cu target. Any bending of crystallographic planes is supposed to cause streaks along the zone axis. However, because a Cu target was used to produce the "white" radiation, wherever the reflection from the characteristic radiation satisfies Bragg's law a strong spot will occur on the streak. The existence of the bent (111) planes indicated that the grown film was highly stressed.

The TLP of an epitaxial β-SiC(100) film grown on a Si(100) substrate and showing characteristic 4-fold symmetry is shown in Fig. IV-22(a).

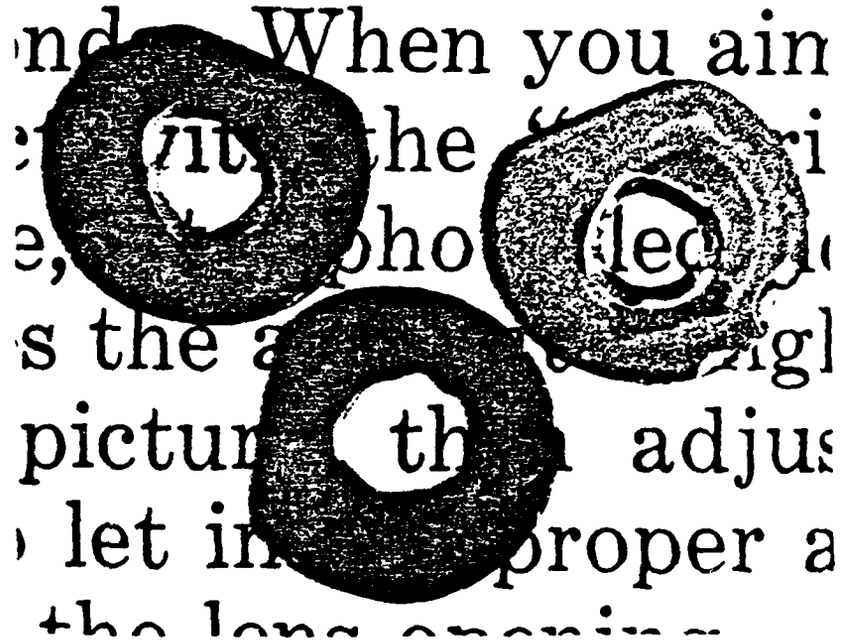

Figure IV-21. The X-ray transmission Laue samples which are epitaxial β-SiC thin films (clear center area) on Si (100) substrates (opaque rings) produced by selectively etching an unwaxed portion of the Si with a mixture of 40v/o HF and 60v/o HNO_3.

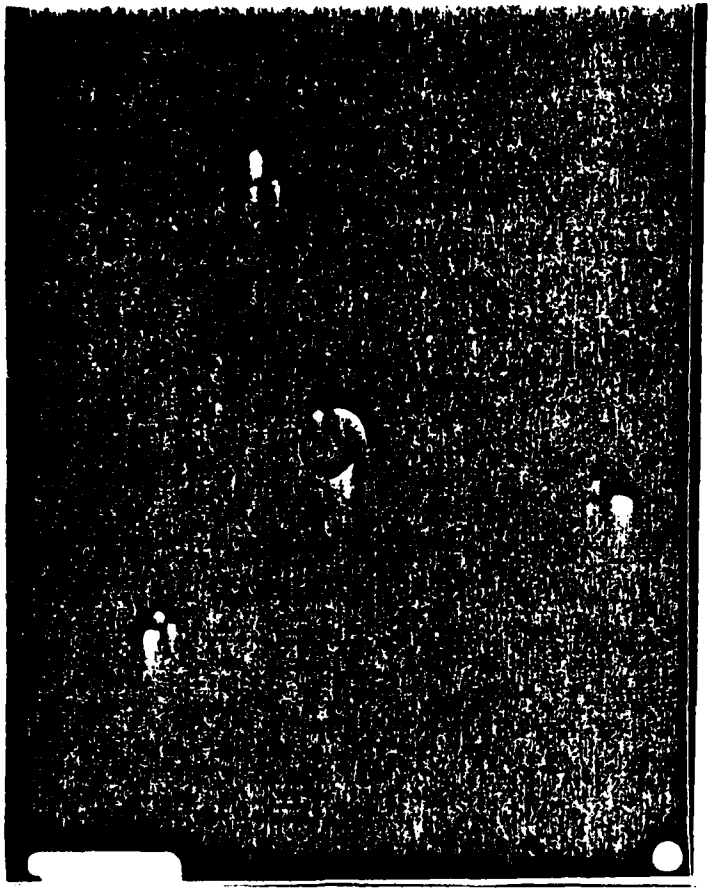

(a)

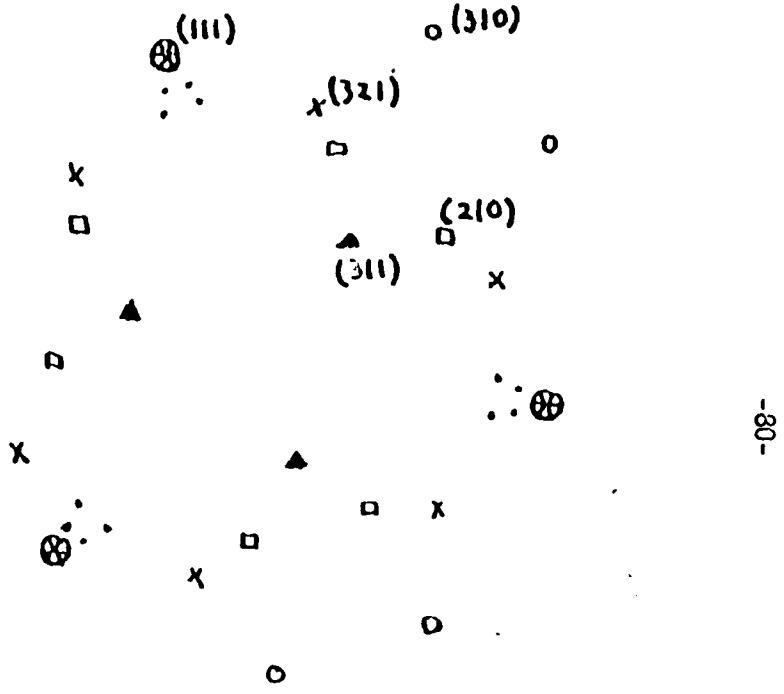

(b)

Figure IV-22. (a) X-ray transmission Laue pattern and (b) the indices of the resulting spots of an epitaxial β-SiC film grown on a Si(111) substrate.

All the Laue spots from the x-ray negative are plotted in Fig. IV-22(b) with their proper indexing. Again, extra spots which could not be routinely indexed were observed very close to the (221) spots. After careful examination, it was determined that the extra spots were on two zone axes and on two rings which correspond to the β-SiC(220) reflextions from the K_α and K_β characteristic radiations of the Cu target. This also indicated the existence of curved planes which formed as a result of stresses in the β-SiC film.

To prove that the extra spots are not caused by the presence of a second phase in the grown film, a Mo x-ray tube was substituted for the Cu tube in order to produce the "white" radiation for the Laue studies. The resulting TLP of the same β-SiC film on the Si(100) substrate is shown in Fig. IV-23. A comparison of this figure with that of Fig. IV-22(a) reveals that both are essentially the same pattern. The important difference is that the extra spots in Fig. IV-22(a) do not occur in the same location as in Fig. IV-23. The extra spots shown in the latter figure are located on four zone axes. Visiable streaks also occur along these zone axes. The wavelength for $Mo_{K\alpha}$ is 0.7107 Å while that for $Mo_{K\beta}$ is 0.6322 Å. Thus, this is proof that the extra spots noted in both Figs. IV-11 and IV-23 were caused by the β-SiC(220) reflections from the characteristic radiations of the Cu and Mo target, respectively, and not by additional phases in the films.

Growth temperature is one of the most important factors which determines the crystallinity of the CVD layers. As shown in Fig. IV-24 (a), the β-SiC film grown on a Si(111) substrate was polycrystalline in nature when the growth temperature was 1070°C. As the temperature of the substrate surface was increased to 1135°C, the grain size became larger, and a number of spot-containing rings were observed on the TED pattern, as shown in Fig. IV-24(b). When the growth temperature was increased to 1360°C, single crystal β-SiC films were obtained, as shown in Fig. IV-24(c). Therefore, it can be concluded that high temperatures are normally required for obtaining epitaxial growth by CVD, particularly on foreign substrates.

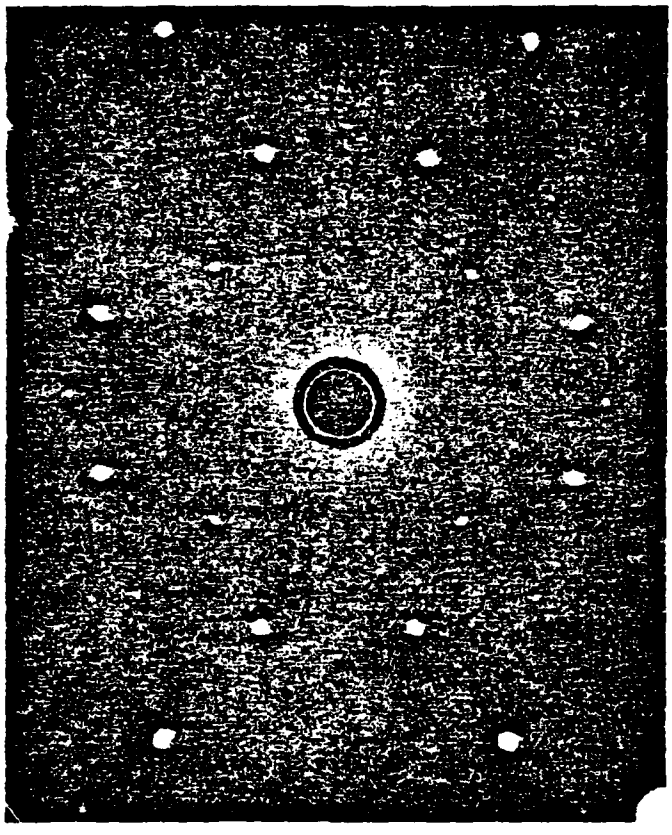

Mo TUBE

Figure IV-23. *X-ray transmission Laue pattern of an epitaxial β-SiC film grown on a Si (100) substrate using a Mo tube to produce the "white" radiation. Note the extra spots as well as streaking along the four zone axes.*

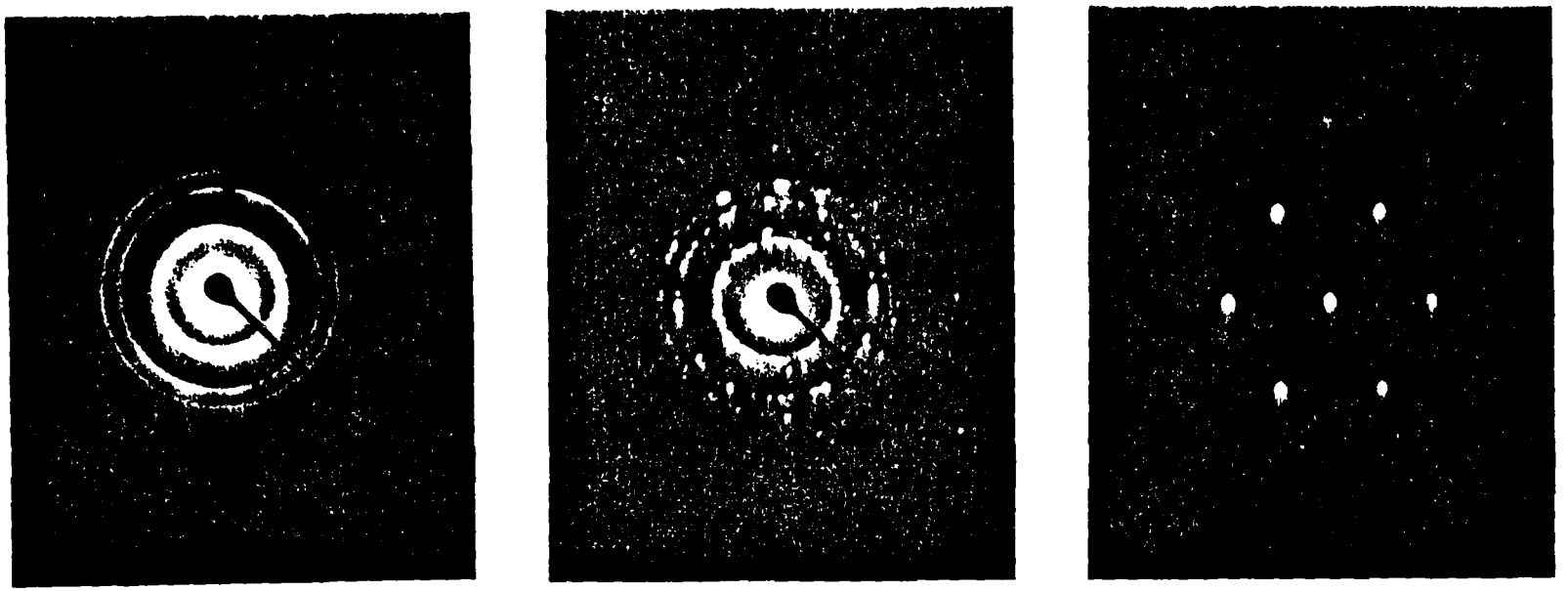

(a) 1070°C (b) 1135°C (c) 1360°C

Figure IV-24. TED patterns of three different β-SiC thin films grown on Si(111) substrates at the given temperatures.

Figure IV-25 shows the same dependence of crystallinity on temperature in the TED patterns for the CVD β-SiC films grown on Si(100) substrates. However, the technique for growing the 1070°C and the 1135°C films was direct CVD; whereas that employed for growing the 1330°C film was chemical conversion followed by CVD. It was very difficult to epitaxially grow single crystalline β-SiC films on Si(100) substrates by the direct CVD method even at a temperature as high as 1360°C.

The crystallinity of the top surface of films grown on Si(111) was also checked by RED at Northeastern University. Figure IV-26 shows the RED pattern obtained at 80 kV electron energy using a camera constant λL = 13.98 Å.

3. Electrical Properties

Table IV-6 lists the electrical properties for the β-SiC(100) epitaxial films having different thickness and measured using the Van der Pauw technique. It is interesting to note that the thinest film has the highest impurity concentration and the lowest mobility. The other two thicker films have very nearly the same Hall mobility. All three films were n-type which may be caused by unintentional doping by N_2. In order to obtain good electrical isolation for the n-type epitaxial layers during the electrical measurements. B-doped p-type Si substrates were employed.

Copper probes mechanically pressed on the β-SiC film surface did not make an ohmic contact to the film. However, Ni probes formed a reasonable good ohmic contact on the n-type β-SiC film surface. After each Van der Pauw measurement, a very thin Ni film was burned into the β-SiC film because of the joule heating effect. This technique can provide a quick and satisfactory way to measure the basic electrical properties of the n-type β-SiC epitaxial films.

C. R-F Sputtering of Thin Films of SiC

There exists a variety of parameters which determine the properties of films during r-f sputtering: anode - to cathode distance, pressure and purity of the carrier gas, peak voltage and power to the cathode,

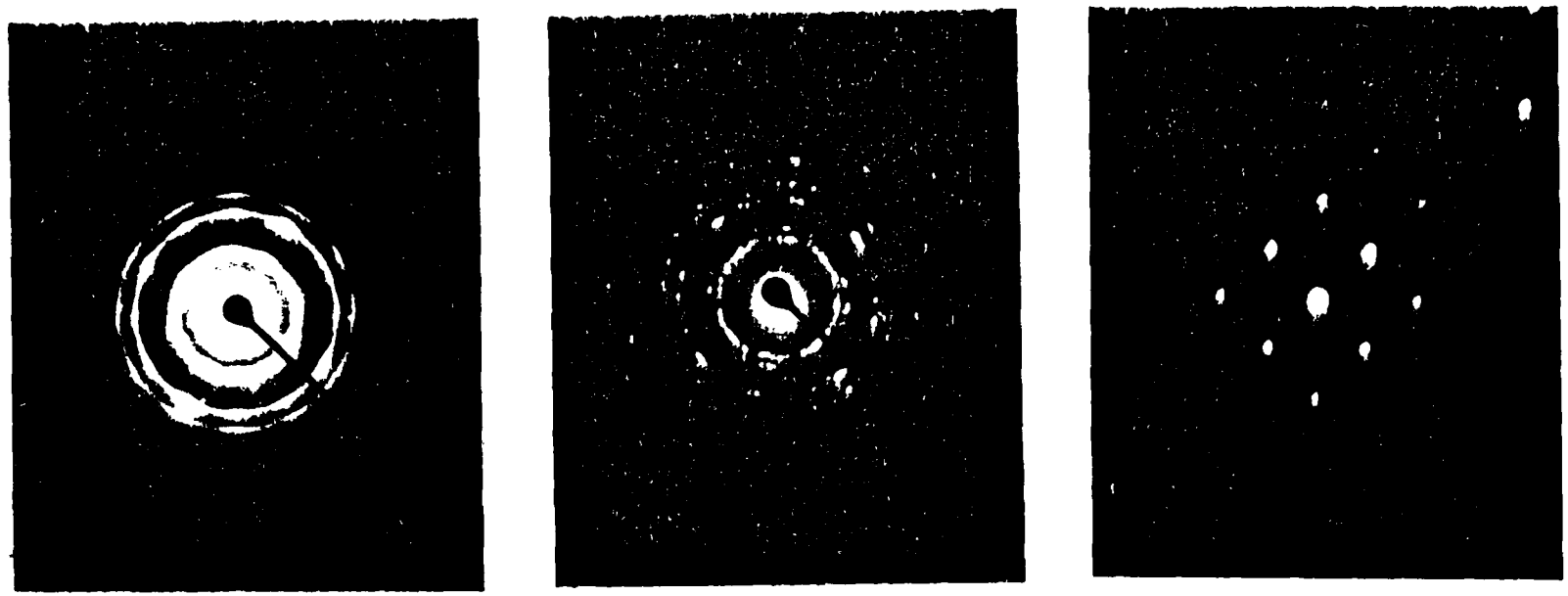

Figure IV-25. TED patterns of three separate β-SiC thin films grown on Si(100) substrates at the given temperatures.

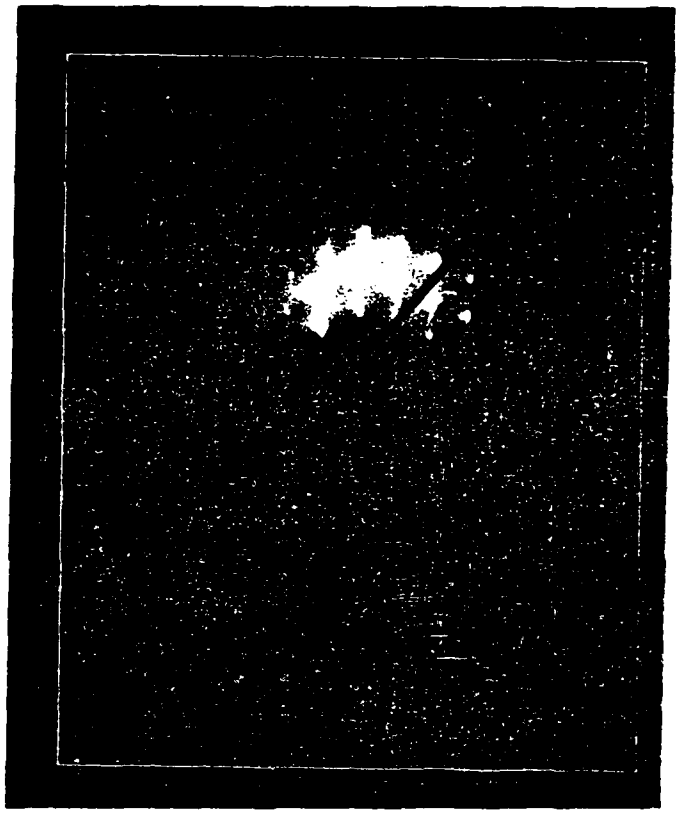

Figure IV-26. RED pattern of an epitaxial β-SiC(111) thin film grown on a Si(111) substrate.

Table IV-6. Electrical properties of n-type β-SiC (100) samples having three different thicknesses and grown on p-type Si(111) substrate.

Sample Number	810916	810917	810919
Epitaxial film thickness (μm)	1.25	5.0	7.5
Resistivity (-cm)	0.13	0.38	0.22
Hall Coefficient	-11.4	-97.4	-59.5
Hall mobility ($cm^2/V.$ sec)	88	256	270
Carrier Conc. (cm^{-3})	$5.5x10^{17}$	$6.4x10^{16}$	$1.1x10^{7}$

substitute temperature, etching conditions and time of deposition, to name a few.

The initial set of conditions employed in our sputtering unit was based on the calculations of Westwood (81) and Anderson, et al. (82) which presented a model for the scattering of sputtered atoms by the sputtering gas at a given power level on the target and at different pressures of the sputtering gas. The distances which atoms travel normal to the target before their energies are thermalized were determined.

The parameters we chose to vary were cathode to anode distance, time of deposition, substrate temperature and the power to the cathode or anode during sputtering or etching, respectively. Prior to each run the Si substrates were masked by several small pieces of Si. This enabled the measurements of film thicknesses and their uniformity by profilometry.

Table IV-3 presents the results of thickness measurements of SiC films sputtered at different experimental conditions. The crystallinity of SiC films was examined by Laue transmission x-ray diffraction and the results show that the deposited films are truly amorphous.

As can be seen from Table IV-7, better uniformity of film thickness was obtained when the substrates were heated during sputtering. At the monitored temperature of 560°C, the uniformity obtained was excellent. The refractive index of the same film was measured by infrared transmittance and the results are presented in Table IV-8.

Table IV-8. The Results of Infrared Transmittance Measurements on Sample 25

λ (nm)	T
2.110	T max
1.745	T min
1.490	T max
1.300	T min

Preparation of film 25: Plasma etch: 500v, 100W 1 hr; sputter: 1180V, 180W, 3.5 hrs, 560°C. P_{Ar} = 13.2 mTorr, Target–Substrate Distance = 2.5 in. In the measurements of refractive index, the determination of film thickness is very important. A short explanation of the calculations is given below

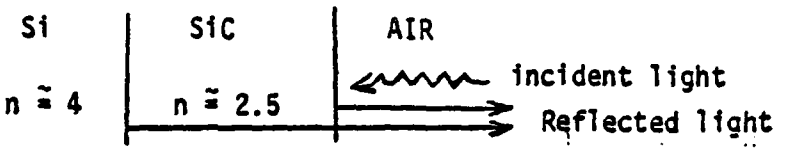

Constructive interference is obtained when the following conditions are satisfied:

Reflected light
$R_{max} = 2nd = m\lambda$
$R_{min} = 2nd = (m + \frac{1}{2})\lambda$

Transmitted light
$T_{max} = 2nd = (m + \frac{1}{2})\lambda$
$T_{min} = 2nd = m\lambda$

where:

λ . . . wavelength of light
n . . . refractive index
d . . . film thickness (1.20μm in this case)
m . . . integer

Table IV-7. The results of thickness measurements of SiC films

Target to Substrate Distance [in]	Argon Pressure mTorr	Plasma etching				Sputtering				Thickness**, +
		Peak Voltage [V]	Power [W]	Time [hr]	T. substr. [°C]	Peak V [V]	Power [W]	Time [hr]	T. Substr. [°C]	[μm]
2.0	9.4	-	-	-	-	1330	150	2	30	0.9 - 1.2
2.0	9.2	-	-	-	-	1300	150	5	30	1.4 - 1.5
2.0	12.9	600	200	1.0	200	1200	200	4	70	0.8 - 1.2
2.5	13.0	-	-	-	-	1150	190	2	65	0.6 - 1.1
2.5	13.0	600	200	0.3	240	1200	200	4	70	0.9 - 1.2
2.5	13.2	500	100	1.0	180	1180	180	3.5	560	1.19 - 1.21
3.0	12.3	500	100	0.6	190	-	-	-	-	0.15 - 0.20

** The thicknesses were measured from the original Si surface to the SiC surface to an accuracy of ± 200Å.

+ For the checking of uniformity, the thicknesses were measured on the center and 2 in. from the anode center in the radial direction.

T max occurs at	λ	m	n_{SiC}	
	2.11	2	2.198	
	1.49	3	2.173	
				$\bar{n} = 2.18$
T min occurs at	1.745	3	2.181	
	1.30	4	2.167	

The measured value of 2.18 for the refractive index is less than the refractive index of either hexagonal or cubic SiC (2.69 or 2.48, respectively (3)). The same effect has been observed for amorphous and crystalline Si, where the refractive index of amorphous Si is about 20% lower than that of crystalline Si. Since Si and SiC have the same crystal structure, the lower measured value of 2.18 for the sputtered films is an additional indication of the non crystallinity of the sputtered films.

The deposited SiC films are yellow and transparent. The color is indicative of their purity; however, neither the purity or the composition has been investigated as yet.

V. Conclusions

1. A state-of-the-art variable pressure barrel-type chemical vapor deposition system has been designed and built in-house in order to grow heteroepitaxial β-SiC thin films on Si substrates.
2. CVD phase diagrams of the Si-C-H and Si-C-Ar system for β-SiC were developed at various total pressures by thermodynamic calculations using "SOLGASMIX-PV" computer program.
3. Direct CVD growth of β-SiC film on Si was difficult and non-reproducible. However, the growth of an epitaxial β-SiC film on Si was reporducible, if a two-step process was employed. This method entails the initial chemical conversion (CC) of the Si surface through the use of C_2H_4 alone. This step is followed by the direct CVD technique in which SiH_4 and C_2H_4 are separately decomposed on the initial converted layer such that a β-SiC thin film is caused to grow.

4. The atomic mass transport mechanism responsible for the conversion is the out-diffusion of Si atoms through the thin as-formed layer(s) and their reaction with C atoms present at the surface as a result of the decomposition of C_2H_4. Characteristic voids (triangular in shape on Si(111) and rectangular in shape on Si(100) in the Si substrate are formed at the interface as a result of this out-diffusion of Si.

5. The surface morphology of the epitaxial β-SiC thin films was influenced by the angle of off-axis orientation of the Si substrates. Results from this study showed that β-SiC films grown on 1° off (100) and 2° off (111) Si wafers are smoother than those grown on 6° off (100) and 4° off (111) wafers, respectively.

6. The epitaxial β-SiC films were transparent and yellow in color. The ranges in various electronic properties of the β-SiC(100) samples measured by the Van der Pauw technique are as follows.

Electronic Properties	Range
Resistivity (ρ)	0.13 - 0.38 Ω-cm
Hall Coeff. (R_H)	(-11.4) - (-97.4)
Mobility (μ)	88 - 270 cm^2/V-sec
Type	n
Carrier Concentration	$6.4x10^{16}$ - $5.5x10^{17}$ cm^{-3}

7. Amorphous films of nominally one micron thickness have been produced by r-f sputtering of a specially prepared high purity CVD SiC target. The deposited films are yellow and transparent. The refractive index of 2.18 is less than that of either the hexagonal or the cubic forms of SiC. This correlates with the x-ray evidence that shows the films to be without long range order.

VI. References

1. S. R. Brinkley, Jr., J. Chem. Phys., 14, 563 (1946).
2. S. R. Brinkley, Jr., ibid., 15, 107 (1947).
3. W. B. White, W. M. Johnson, and G. B. Dantzig, ibid., 28, 751 (1958).
4. T. J. Lewis, Mat. Res. Bull., 4,S321 (1969).
5. S. Minagawa and H. C. Gatos, Jap. J. Appl. Phys., 10, 844 (1971).
6. D. R. Cruise, J. Phys. Chem., 68, 3797 (1964).

7a. J. M. Harris, H. C. Gatos, and A. F. Witt, J. Electrochem. Soc., 116, 380 (1969).

b. J. M. Harris, H. C. Gatos, and A. F. Witt, ibid, 118, 338 (1971).

8. G. Eriksson, Acta Chem. Scand., 25, 2651 (1971).
9. G. Eriksson and E. Rosén, Chemica Scripta, 4, 193 (1973).
10. G. Eriksson, ibid., 8, 100 (1975).
11. T. M. Bessman and K. E. Spear, J. Electrochem. Soc., 124, 786 (1977).
12. R. W. Brander, in Silicon Carbide - 1973, Ed. by R. C. Marshall., J. W. Faust, Jr., and C. E. Ryan, University of South Carolina Press, Columbia, South Carolina (1974).
13. J. Schlichting, Powder Metall. Int., 12, 141 (1980).
14. W. G. Spitzer, D. A. Kleinman, and C. J. Frosch, Phys. Rev., 113, 133 (1959).
15. H. Nakasima, T. Sugano, and H. Yanai, Jap. J. Appl. Phys., 5, 374 (1966).
16. J. Graul and E. Wagner, Appl. Phys. Lett., 21, 67 (1972).
17. M. Balog, A. Reisman, and M. Berkenblit, J. Elec. Mat., 9, 669 (1980).
18. J. Mercier and C. Roussel, 3rd Int. Conf. on CVD, p 426 (1972).
19. I. H. Khan and R. N. Summergrad, Appl. Phys. Lett., 11, 12 (1967).
20. I. H. Khan, Mat. Res. Bull., 4, S285 (1969).
21. A. S. Brown and B. E. Watts, J. Appl. Cryst., 3, 172 (1970).
22. A. J. Learn and I. H. Khan, Thin Solid Films, 5, 145 (1970).

AD-A118 800 NORTH CAROLINA STATE UNIV RALEIGH DEPT OF MATERIALS --ETC F/G 20/2
SINGLE CRYSTAL EPITAXY AND CHARACTERIZATION OF BETA-SIC.(U)
JUL 82 R F DAVIS N00014-79-C-0121
UNCLASSIFIED 243-027-013 NL

2 OF 2
AD A
118800

END
DATE FILMED
09-82
DTIC

23. K. E. Haq and I. H. Khan, J. Vac. Sci. Technol., 7, 490 (1970).

24. C. J. Mogab and H. J. Leamy, J. Appl. Phys., 45, 1075 (1974).

25. L. Meyer and R. Gomer, Third Biannual Carbon Conference, Buffalo, N. Y. (1957).

26. N. C. Tombs, J. J. Comer, and J. F. Fitzgerald, Solid State Elec., 8, 839 (1965).

27. A. Reisman, IBM T. J. Watson Research Center, Personal Communication (1981).

28. R. W. Bartlett and R. A. Mueller, Mat. Res. Bull., 4, S341 (1969).

29. M. J. Noone and J. P. Roberts, Nature, 212, 71 (1966).

30. T. D. Gulden, J. Amer. Cera. Soc., 51, 424 (1968).

31. N. Setaka and Z. Inone, ibid., 52, 624 (1969).

32. R. J. Price, Cera. Bull., 48, 859 (1969).

33. A. W. C. Van Kemenade and C. F. Stemfoort, J. Crystal Growth, 12, 13 (1972).

34. J. Chin, P. K. Gantzel, and R. G. Hudson, Thin Solid Films, 40 57 (1977).

35. P. Rai-Choudhury and N. P. Formigoni, J. Electrochem. Soc., 116, 1440 (1969).

36. K. A. Jacobson, ibid, 118, 1001 (1971).

37. J. T. Kendall and D. Yeo, Proc. Intern. Congr. Applied Chem. 11th, London 1947, Vol. I: Inorganic and Geochemistry, Physical Chemistry, p 171 (1950).

38. I. Berman, C. E. Ryan, R. C. Marshall, and J. R. Littler, "The Influence of Annealing on Thin Films of Beta SiC," AFCRL-72-0737 (1972).

39. S. Nishino, Y. Hazuki, H. Matsunami, and T. Tanaka, J. Electrochem. Soc., 127, 2674 (1980).

40. J. E. Spruiell, "Chemical Vapor Deposition of Silicon Carbide from Silicon Tetrachloride-Methane-Hydrogen Mixtures," ORNL-4326 (1968).

41. D. M. Jackson, Jr. and R. W. Howard, Trans. Met. Soc. AIME, 233, 468 (1965).

42. S. Nishino, H. Matsunami, and T. Tanaka, Jap. J. Appl. Phys., 14, 1833 (1975).

43. H. Matsunami, S. Nishino, and T. Tanaka, J. Crystal Growth, 45, 138 (1978).

44. K. E. Bean and P. S. Gleim, J. Electrochem. Soc., 114, 1158 (1967).

45. N. Setaka and K. Ajiri, J. Amer. Cera. Soc., 55, 540 (1972).

46. K. Kuroiwa and T. Sugano, J. Electrochem. Soc., 120, 138 (1973).

47. J. J. Nickl and C. V. Braunmühl, J. Less-Common Metals, 37, 317 (1974).

48. H. Matsunami and S. Nishino, Private Communication (1981).

49. I. Berman, R. C. Marshall, and C. E. Ryan, Silicon Carbide 1973, pp 42 and 593 (1974).

50a. A. J. Learn and K. E. Haq, Appl. Phys. 40, 430 (1969).

b. A. J. Learn and K. E. Haq, Appl. Phys. Lett. 17, 26 (1970).

51. K. E. Haq, Appl. Phys. Let. 26, 255 (1975).

52. Yu. M. Tairov and V. F. Tsvetkov, J. Cryst. Grow., 52, 146 (1981).

53. S. Nishino, Y. Hazuki, H. Matsunami, and T. Tanaka, J. Electrochem. Soc., 127, 2674 (1980).

54. JANAF Thermochemical Tables (a) Second Edition, NSRDS-NBS 37, National Bureau of Standards, USA (1971), (b) 1974 Supplement, J. Phys. Chem. Ref. Data 3, pp 311-480 (1974), (c) 1975 Supplement, J. Phys. Chem. Ref. Data 4 [1], pp 1-175 (1975).

55. Selected Values of the Thermodynamic Properties of the Elements, eds R. Hultgren, P. D. Desai, D. T. Hawleins, M. Gleiser, and K. K. Kelley, American Society for Metals, Ohio (1973).

56. A. Addamiano and L. S. Staikoff, "Stabilization of Cubic Silicon Carbide," J. Phys. Chem. Solids 26 [4], 669-672 (1965).

57. A. R. Kieffer, P. Ettmayer, E. Angel, and A. Schmidt, "Phase Stability of Silicon Carbide in the Ternary System Si-C-N," Mater. Res. Bull., 4, S153-S166 (1969).

58. N. W. Jepps and T. F. Page, "The 6H → 3C 'Reverse' Transformation in Silicon Carbide Compacts," Commun. Am. Ceram. Soc. 64 [12], C177-C178 (1981).

59. C. E. Ryan, R. C. Marshall, J. J. Hawley, I. Berman, and D. P. Considine, "The Conversion of Cubic to Hexagonal Silicon Carbide as a Function of Temperature and Pressure," AFCRL-67-0436 (Air Force Cambridge Research Laboratories), August 1967.

43. H. Matsunami, S. Nishino, and T. Tanaka, J. Crystal Growth, 45, 138 (1978).

44. K. E. Bean and P. S. Gleim, J. Electrochem. Soc., 114, 1158 (1967).

45. N. Setaka and K. Ajiri, J. Amer. Cera. Soc., 55, 540 (1972).

46. K. Kuroiwa and T. Sugano, J. Electrochem. Soc., 120, 138 (1973).

47. J. J. Nickl and C. V. Braunmühl, J. Less-Common Metals, 37, 317 (1974).

48. H. Matsunami and S. Nishino, Private Communication (1981).

49. I. Berman, R. C. Marshall, and C. E. Ryan, Silicon Carbide 1973, pp 42 and 593 (1974).

50a. A. J. Learn and K. E. Haq, Appl. Phys. 40, 430 (1969).

b. A. J. Learn and K. E. Haq, Appl. Phys. Lett. 17, 26 (1970).

51. K. E. Haq, Appl. Phys. Let. 26, 255 (1975).

52. Yu. M. Tairov and V. F. Tsvetkov, J. Cryst. Grow., 52, 146 (1981).

53. S. Nishino, Y. Hazuki, H. Matsunami, and T. Tanaka, J. Electrochem. Soc., 127, 2674 (1980).

54. JANAF Thermochemical Tables (a) Second Edition, NSRDS-NBS 37, National Bureau of Standards, USA (1971), (b) 1974 Supplement, J. Phys. Chem. Ref. Data 3, pp 311-480 (1974), (c) 1975 Supplement, J. Phys. Chem. Ref. Data 4 [1], pp 1-175 (1975).

55. Selected Values of the Thermodynamic Properties of the Elements, eds R. Hultgren, P. D. Desai, D. T. Hawleins, M. Gleiser, and K. K. Kelley, American Society for Metals, Ohio (1973).

56. A. Addamiano and L. S. Staikoff, "Stabilization of Cubic Silicon Carbide," J. Phys. Chem. Solids 26 [4], 669-672 (1965).

57. A. R. Kieffer, P. Ettmayer, E. Angel, and A. Schmidt, "Phase Stability of Silicon Carbide in the Ternary System Si-C-N," Mater. Res. Bull., 4, S153-S166 (1969).

58. N. W. Jepps and T. F. Page, "The 6H → 3C 'Reverse' Transformation in Silicon Carbide Compacts," Commun. Am. Ceram. Soc. 64 [12], C177-C178 (1981).

59. C. E. Ryan, R. C. Marshall, J. J. Hawley, I. Berman, and D. P. Considine, "The Conversion of Cubic to Hexagonal Silicon Carbide as a Function of Temperature and Pressure," AFCRL-67-0436 (Air Force Cambridge Research Laboratories), August 1967.

60. S. Minagawa and H. C. Gatos, "Equilibrium Computation for the Growth of Alpha Silicon Carbide from Silicone and Propane in the Presence of Hydrogen or an Inert Gas," Jap. J. Appl. Phys. 19 [7] pp 844-849 (1971).

62. R. F. Lever, "The Equilibrium Behaviour of the Silicon-Hydrogen-Chlorine System," IBM J. 8 [4] pp 460-465 (1964).

63. M. Turpin and A. Robert, "Structure of SiC Ribbons and Continuous Fibres grown by Chemical Vapour Deposition," Proc. Brit. Ceram. Soc., No. 22, pp 337-353 (1973).

64. F. Christin, R. Naslain, and C. Bernard, "A Thermodynamic and Experimental Approach of Silicon Carbide - CVD Application to the CVD - Infiltration of Porous Carbon-Carbon Composites," pp 499-514 in Proceedings of the Seventh International Conference on Chemical Vapor Deposition, 1979, eds T. O. Sedgwick and H. Lydtin, The Electrochemical Society, Princeton, New Jersey (1979).

65. R. Pampuch and L. Stobierski, "Morphology of Silicon Carbide Formed by Chemical Vapor Deposition," pp 180-190, in Proceedings of the 3rd CIMTEC: 3rd International Meeting on Modern Ceramics Technologies, (Rimini, Italy, May 27-31, 1976) ed P. Vincenzini, National Research Council, Faenze, 1978.

66. B. Wessels, H. C. Gatos, and A. F. Witt, "Epitaxial Growth of Silicon Carbide by Chemical Vapor Deposition," pp 25-32 in Silicon Carbide - 1973 (see Ref. 2).

67. P. Popper and F. L. Riley, "The Texture of Pyrolyfic Silicon Carbide," Proc. Brit. Ceram. Soc. No. 7, pp 99-109 (1967).

68. Y. Avigal, M. Schieber, and R. Levin, "The Growth of Hetero-epitaxial SiC Films by Pyrolysis of Various Alkyl-Silicon Compounds," J. Crystal Growth 24/25, pp 188-192 (1974).

69. J. M. Harris, H. C. Gatos, and A. F. Witt, "Growth Characteristics of Alpha Silicon Carbide. I. Chemical Vapor Deposition," pp 795-798, eds J. M. Blocher and J. C. Withers, Electrochemical Society, New York, 1970.

70. R. W. Brander, "Epitaxial Growth of SiC Layers," pp 8-23 in Silicon Carbide - 1973 (see Ref. 2).

71. F. Kobayashi, K. Ikawa, and K. Iwamoto, "Formation of Carbon-Excess SiC from Pyrolysis of CH_3SiCl_3," J. Crystal Growth 28, 395-396 (1975).

72. T. D. Gulden, "Deposition and Microstructure of Vapor-Deposited Silicon Carbide," J. Am. Ceram. Soc. 51 [8] pp 424-427 (1968).

73. W. von Muench and E. Pettenpaul, "Preparation of Pure and Doped Silicon Carbide by Pyrolysis of Silane Compounds," J. Electrochem. Soc. 125 [2], pp 294-299 (1978).

74. J. Chin, P. K. Gantzel, and R. G. Hudson, "The Structure of Chemical Vapor Deposited Silicon Carbide," Thin Solid Films 40, pp 57-72 (1977).

75. J. R. Weiss and R. J. Diefendorf, "Chemically Vapor Deposited SiC for High Temperature and Structural Applications," pp 80-91, in Silicon Carbide - 1973 (see Ref. 2).

76. L. M. Ivanova, G. A. Kazaryan, and A. A. Pletyushkin, "The Preparation of Silicon Carbide by the Thermal Decomposition of Methylchlorosilane Vapors," Inorg. Mater. (Engl. Transl.) 2 [2], pp 192-196 (1966).

77. P. Rai-Choudhury and N. P. Formigoni, "β-Silicon Carbide Films," J. Electrochem. Soc., 116 [10] pp 1440-1443 (1969).

78. C. Bernard, "The Application of Thermodynamics to Chemical Vapor Deposition Processes," pp 3-16 in Proceedings of the Eighth International Conference on Chemical Vapor Deposition, 1981, eds J. M. Blocher, Jr., G. E. Vuillard, and G. Wahl, The Electrochemical Society, Pennington, New Jersey (1981).

79. R. Colmet, R. Naslain, P. Hagenmuller, and C. Bernard, "Thermodynamic and Experimental Analysis of Chemical Vapor Deposition of Alumina from $AlCl_3$-H_2-CO_2 Gas Phase Mixtures," pp 17-31 in Proceedings of the Eighth International Conference on Chemical Vapor Deposition, 1981, eds J. M. Blocher, Jr., G. E. Vuillard, and G. Wahl, The Electrochemical Society, Pennington, New Jersey (1981).

80. K. F. Spear, "Applications of Phase Diagrams and Thermodynamics to CVD." pp 1-16 in Proceedings of the Seventh International Conference on Chemical Vapor Deposition, 1979, eds T. O. Sedgwick and H. Lydtin, The Electrochemical Society, Princeton, New Jersey (1979).

81. W. D. Westwood, J. Vac. Sci. Technol. 15, 1 (1978).

82. D. A. Anderson, G. Moddel, M. A. Paesler and William Paul, J. Vac. Sci. Technol. 16, 906 (1979).

DISTRIBUTION LIST - TECHNICAL REPORTS

CONTRACT N00014-79-C-0121

Office of Naval Research (4)
Code 426Y
800 North Quincy Street
Arlington, VA 22217

Naval Research Laboratory
4555 Overlook Avenue, S.W.
Washginton, DC 20375
Attn: Code 6812 (1)
6820 (2)

Defense Documentation Center (12)
Building 5, Cameron Station
Alexandria, VA 22314

Dr. Y. S. Park (1)
AFAL/DHR
Building 450
Wright-Patterson AFB
Ohio 45433

ERADCOM (1)
DELET-M
Fort Monmouth, NJ 07703

Dr. Larry Flesner (1)
Naval Ocean Systems Center
Code 922
271 Catalina Blvd.
San Diego, CA 9215?

Dr. William Lindley (1)
MIT
Lincoln Laboratory
124A, P.O. Box 73
Lexington, MA 02173

Mr. Sven Roosild (1)
DARPA/DSO
1400 Wilson Blvd
Arlington, VA 22209

Commander (1)
U.S.Army Electronics Command
V. Gelnovatch
(DRSEL-TL-IC)
Forth Monmouth, NJ 07703

Commandant (1)
Marine Corps
Scientific Advisor (Code AX)
Washington, DC 20380

Commander, AFAL (1)
AFAL/DHM
Mr. Richard L. Remski
Wright-Patterson AFB, OH 45433

Professor Walter Ku (1)
Phillips Hall
Cornell University
Ithaca, NY 14853

Commander (1)
Harry Diamond Laboratories
Mr. Horst W. A. Gerlach
2800 Powder Mill Road
Adelphia, MD 20783

Advisory Group on Electron Devices (1)
201 Varick Street, 9th Floor
New York, NY 10014

Professor L. Eastman (1)
Phillips Hall
Cornell University
Ithaca, NY 14853

Professors Hauser and Littlejohn (1)
Department of Electrical Engr.
North Carolina State University
Raleigh, NC 27650

Dr. R. S. Feigelson (1)
Center for Materials Research
Stanford University
Stanford, CA 94305

Dr. Y. Kim (1)
ONR Scientific Liaison Group
American Embassy
A.P.O. San Francisco 96503

Dr. H. M. Manasevit (1)
Rockwell International
P. O. Box 3105
Dept. 527
Mail Stop HA-22
Anaheim, CA 92803

Enclosure (1)


ATE
LME